Review

Application of Biochar as Functional Material for Remediation of Organic Pollutants in Water: An Overview

Mohamed Faisal Gasim [1], Zheng-Yi Choong [1], Pooi-Ling Koo [1], Siew-Chun Low [2], Mohamed-Hussein Abdurahman [2], Yeek-Chia Ho [3,*], Mardawani Mohamad [4], I Wayan Koko Suryawan [5], Jun-Wei Lim [6] and Wen-Da Oh [1,*]

1 School of Chemical Sciences, Universiti Sains Malaysia, Gelugor 11800, Penang, Malaysia; mohamed.faisal@student.usm.my (M.F.G.); choongzhengyi599@student.usm.my (Z.-Y.C.); pooiling0101@student.usm.my (P.-L.K.)
2 School of Chemical Engineering, Engineering Campus, Universiti Sains Malaysia, Seri Ampangan, Nibong Tebal 14300, Pulau Pinang, Malaysia; chsclow@usm.my (S.-C.L.); mohamed@student.usm.my (M.-H.A.)
3 Centre for Urban Resource Sustainability, Civil and Environmental Engineering Department, Institute of Self-Sustainable Building, Universiti Teknologi PETRONAS, Seri Iskandar 32610, Perak Darul Ridzuan, Malaysia
4 Faculty of Bioengineering and Technology, Jeli Campus, Universiti Malaysia Kelantan, Jeli 17600, Kelantan, Malaysia; mardawani.m@umk.edu.my
5 Department of Environmental Engineering, Faculty of Infrastructure Planning, Universitas Pertamina, Komplek Universitas Pertamina, Jalan Sinabung II, Terusan Simprug, Jakarta 12220, Indonesia; i.suryawan@universitaspertamina.ac.id
6 Department of Fundamental and Applied Sciences, HICoE-Centre for Biofuel and Biochemical Research, Institute of Self-Sustainable Building, Universiti Teknologi PETRONAS, Seri Iskandar 32610, Perak Darul Ridzuan, Malaysia; junwei.lim@utp.edu.my
* Correspondence: yeekchia.ho@utp.edu.my (Y.-C.H.); ohwenda@usm.my (W.-D.O.)

Abstract: In recent years, numerous studies have focused on the use of biochar as a biological material for environmental remediation due to its low-cost precursor (waste), low toxicity, and diversity of active sites, along with their facile tailoring techniques. Due to its versatility, biochar has been employed as an adsorbent, catalyst (for activating hydrogen peroxide, ozone, persulfate), and photocatalyst. This review aims to provide a comprehensive overview and compare the application of biochar in water remediation. First, the biochar active sites with their functions are presented. Secondly, an overview and summary of biochar performance in treating organic pollutants in different systems is depicted. Thereafter, an evaluation on performance, removal mechanism, active sites involvement, tolerance to different pH values, stability, and reusability, and an economic analysis of implementing biochar for organic pollutants decontamination in each application is presented. Finally, potential prospects to overcome the drawbacks of each application are provided.

Keywords: biochar; adsorption; H_2O_2 activation; O_3 activation; peroxymonosulfate activation; peroxydisulfate activation; photocatalysis; organic pollutants

1. Introduction

Over the past few years, the rapid growth of various industries has led to the release of toxic pollutants to the environment. In particular, various refractory pollutants such as antibiotics, phenolic compounds, dyes, and heavy metals are detected in numerous water bodies and soil [1–5]. In particular, pollution due to refractory pollutants in water bodies is of emerging concern due to its greater mobility compared to soil. While these pollutants pose a threat to public health, they also disrupt the microbial ecosystem [6,7]. For instance, the release of trace antibiotics will lead to the development of multidrug-resistant strains, which will result in less effective clinical treatment effects of conventional antibiotics [7]. Phenolic compounds such as chlorophenols are toxic and may induce

carcinogenic and mutagenic effects. In order to alleviate this problem, methods such as adsorption [8], membrane separation [9], and advanced oxidation processes (AOPs) [10] can be used to treat the wastewater before it is discharged into the environment. Generally, adsorption and membrane separation involve the separation of pollutants and water without destroying the pollutants, while AOPs utilizes reactive oxygen species (ROS) generation for organics mineralization.

Recently, biochar has gained attention in various environmental remediation applications. Biochar can be obtained by the direct carbonization of organic wastes in an oxygen-deficient environment. Compared with other carbon-based materials, some of the advantages of using biochar for environmental remediation include low production cost (cheap raw materials), relatively simple preparation methods (facile pyrolysis of biomass), and eco-friendly (waste recovery). Furthermore, the properties of biochar can be engineered more easily (compared with other carbon allotropes) by changing the synthesis parameters (e.g., synthesis temperature and duration) [11,12], careful selection of biomass as a precursor [13], and functionalization (e.g., heteroatom doping, oxygen tuning, and defects) [14,15].

Numerous reviews on the use of biochar in specific environmental applications are available [16–22], howbeit, with modest emphasis on comparing biochar performance and the mechanism of treating organic pollutants under different systems for finding superior applications of biochar and to fully realize its potential. For instance, Dai et al. [21] discussed the employment of biochar as an adsorbents for organic pollutants, however, without discussing biochar potential in other pollutant remediation systems. Similarly, Zhou et al. [19] and Zhao et al. [23] reviewed biochar as AOPs catalyst and persulfate activator, respectively, without comparison against other systems (e.g., adsorption, O_3 activation). Herein, we attempt to ascertain the superlative application of biochar in the environmental decontamination of organic pollutants, particularly adsorption and AOPs, including hydrogen peroxide (H_2O_2) activation, ozone (O_3) activation, persulfate (PS) activation, and photocatalysis. At first, this review provides information on the numerous properties and active sites of biochar that contribute to wastewater purification. Thereafter, an overview of biochar materials performance in several application is presented. Then, different applications were compared in terms of performance efficiency, removal mechanism of organics matter, resistance to changes in water pH, durability of biochar, and cost factors, along with the limitations of each application were determined. Finally, the brief prospects to overcome these limitations are elucidated.

2. Biochar Active Sites and Characteristics

Biochar is mainly composed of carbon, oxygen, heteroatoms (i.e., N, S), and minerals (Na, C, K). The composition distribution is highly dependent on the biochar precursor and the synthesis conditions and hence varies significantly from one biochar to another. For instance, lignin-rich (lignocellulosic) biomass sources generally yield highly carbonized and graphitized biochar materials, whereas non-lignocellulosic biomass-derived biochar will be enriched with inorganic species. For example, rice husk (contains 15–17% of silica [24]) derived biochar will encompass high Si content, whilst biomass sources such as fish bone and human hair will endow the corresponding biochar with heteroatomic species (i.e., N and S) [22,25,26]. Moreover, the surface area and active sites are influenced with biomass selection. For example, PFRs formation is related to lignin content in biomass [20], while the cellulose content in biomass is proportionally related with high surface area and porosity levels [27]. Additionally, the manipulation of biochar synthesis temperature will affect the content and composition of biochar. Higher pyrolysis temperatures will increase the graphitic carbon content via carbonization and graphitization while lowering oxygen and hydrogen contents along with enhancing the porous structure of the biochar [28–30].

The main active sites of biochar include oxygen-functional groups (OFGs), sp^2 hybridized carbon, heteroatoms (i.e., N, S, P, B), and PFRs. Biochar generally has a relatively large specific surface area (SSA) with high porosity to host these active sites for envi-

ronmental applications. The electron-rich OFGs, such as the ketonic (C=O) group, can mediate the catalytic reaction with the oxidant, involving the production of ROS [31]. The sp.^{2}-hybridized carbon can provide electron-rich sites for adsorption and catalysis. The addition of foreign species such as heteroatoms (particularly S, N, B, and P) into the biochar carbon lattice can endow it with functional active sites. Due to its matching atomic radius yet different electronegativity, N is the prevalent heteroatom in doping biochar, especially for catalysis [30,32]. Heteroatoms can be doped into the biochar either from an endogenous source (biomass) or exogenously. Meanwhile, PFRs can act as an activator by facilitating the generation of free radicals in oxidant-containing systems [33]. PFRs can exist in biochar in three statuses: oxygen-centered, carbon-centered, and carbon-centered PFRs with OFGs [34].

Since carbon atoms are the building blocks of biochar (>65% carbon content [35]), understanding the carbon structural characteristics in biochar is of paramount importance for the successful utilization of biochar in environmental applications. These characteristics encompass graphitization and carbon hybridization status, defective degree, and aromaticity. The degree of graphitization can be interpreted as the extent of similarity between the studied biochar and graphene. The graphitized biochar structure allows π-π electron donor–acceptor (EDA) interactions with organics [36]. In addition, the extensive conjugation of sp.^{2}-hybridized carbons furnishes the biochar with excellent electrical conductivity and enhanced electron transfer capability through the carbon structure [37]. As for the hybridization status, the co-existence of sp.^{2}/sp.^{3} hybridization can have a positive effect on biochar activity, particularly by promoting an internal electron flow from the sp.^{3}-carbon (donor) to sp.^{2}-carbon (acceptor), which is followed by an external electron migration from the later carbon configuration to oxidants [36,38]. Meanwhile, the formation of defective sites (i.e., edge defects, vacancies, curvatures) can destroy the stability of the graphitized structure and provide superior electron-donating capacity for defective biochar. Typically, the graphene-like structure is composed of carbon layers, in which each carbon atom is covalently bonded to three adjacent carbon atoms by three electrons. As a result of its half-filled orbital, the final fourth valence electron forming π-bonds is delocalized and unconfined from movement through the carbon structure. These delocalized π-electrons prefer to migrate and form dangling σ-bonds states at the edges and defects [36,39] to fill in the missing carbon atom at these sites. Dangling σ-bonds with delocalized π-electrons at the defects will foster the electron transfer process from the edged carbon for catalysis reactions. The degree of aromaticity is the extent of aromatic carbon presence with respect to the total carbon within the biochar. The aromatic structure of biochar serves the following functions: (i) π-electrons in the conjugated aromatic system supply the biochar with enhanced electrical conductivity [28], (ii) enriches the biochar with π-π* transitions in the aromatic rings, promoting a positive effect on catalysis [40], (iii) the conjugated π-aromatic structure can act as electron-donating moieties [41] to enhance the catalytic performance, and (iv) the aromatic structure can provide resistance to undesirable oxidative and cannibalistic reactions on the biochar surface (unlike alkyl moieties), which can improve the durability of the active sites.

3. Applications of Biochar in Environmental Remediation

3.1. Adsorption

Adsorption is a common technique to remove organic pollutants. Due to its relatively low operational cost, adsorption is widely utilized for water remediation. Table 1 presents an overview of the performance of biochar as an adsorbent for various organic pollutants. The criteria for an effective adsorbent include having high SSA and porosity along with the abundance of active sites. Generally, the adsorption process relies on the liquid–solid intermolecular attraction between the adsorbate and the adsorbent, which leads to the accumulation of solute molecules on the adsorbent surface [42]. The adsorption mechanisms between the biochar and organic pollutant occur through physical and chemical interactions, including H-bonding, hydrophobic interactions, electrostatic attraction,

π-π EDA interactions, complexes adsorption, Lewis acid–base interactions, pore filling, partition uncarbonized fraction, dipole–dipole interactions, Coulombic attraction, spectrometer exchange, and acceptor interactions [22]. The adsorption process undertaken is controlled by the nature of the adsorbate, biochar properties, and operational condition (i.e., pH, pressure of water matrix, rate). The adsorption process is divided into three stages. First, there is external mass transfer of organic pollutants from the aqueous solution to the biochar surface (external diffusion), which is followed by the diffusion of organic molecules into the pores of biochar (internal diffusion) and ending with the adsorptive interactions (Figure 1) [14,43].
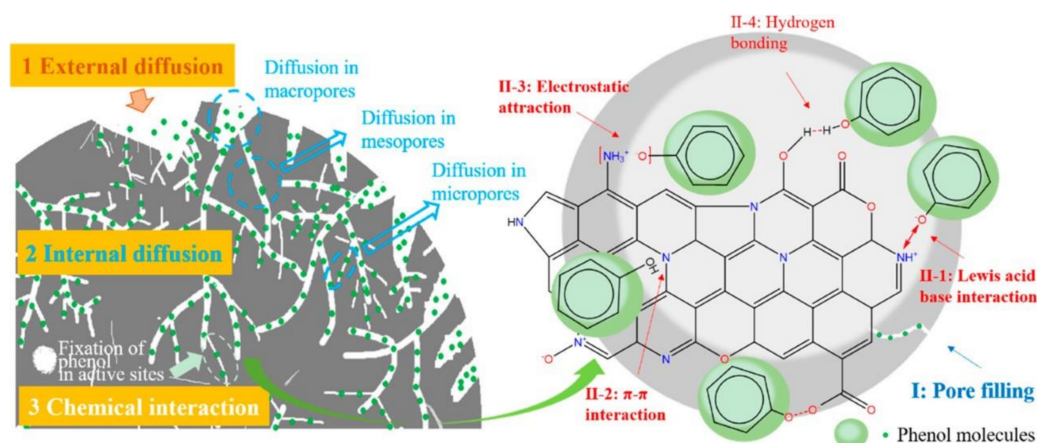

Figure 1. Mechanism of phenol adsorption by N-doped biochar. Reprinted with permission from Li et al. [14]. Copyright 2019 American Chemical Society.

Generally, OFGs can promote the adsorption of organics by various mechanisms viz, H-bonding, ion exchange, π-π interactions, and Coulombic attraction [44]. For example, OFGs on the biochar surface can promote rapid chemisorption via H-bonding with -OH groups of the organic pollutant as the -OH groups serve as a H-donor [45]. For H-bonding, whether present on the biochar surface or organic pollutant, groups such as -NH and -OH serve as H-donors, whilst groups such as benzene rings, F, N, and O act as H-acceptors for H-bonding. In addition, the presence of -OH and -COOH on the surface of biochar makes it more hydrophilic, thereby promoting hydrophobic interactions with organic pollutants with a high level of hydrophobicity. On the other hand, pollutants with strong electron withdrawing functional groups (i.e., F, N-heteroaromatic rings) acting as electron acceptors can allow the adsorption processes of encompassed π-π EDA interaction with biochar [46]. Carbon structural properties may also participate in the adsorption process. The graphitic carbon structure promotes the adsorption of organics. Particularly, the adsorption process takes place between the highly graphitized carbon layers and the aromatic structure of the pollutant through π-π interactions because the graphitized biochar will act as an excellent π-electron donor, and the pollutant will act as an acceptor. For instance, Kim et al. [36] studied the effect of pyrolysis temperature on the adsorption and catalytic activity of biochar from apple tree pruning waste for the removal of ACT. Considering the ACT pKa (9.4) and its log K_{ow} (0.46) with the adsorption reaction taking place at a medium pH value (5.9–6.1), both electrostatic attractions and hydrophobic interactions between the biochar and ACT were not the reason for the enhanced adsorption efficiency. Consequently, it was concluded that the enhanced adsorption was ascribed to the π-π EDA interactions, especially that the enhancement in the adsorption was in good agreement with the enhancement of the graphitization degree of the synthesized biochar. Similarly, the maximum adsorption (32.9%) of sulfamethoxazole (SMX) by *Spirulina* residue-derived biochar (SDBC 900) was ascribed to enhanced graphitization inducing greater π-π interactions between the carbon surface and the SMX aromatic rings [29]. Heteroatoms can enhance the adsorption efficiency of biochar. For instance, biochar derived from peanut shells can only remove 20% of diethyl phthalate, while co-doping with N and S allowed 60% of the same pollutant to

be removed [47]. N doping can alter the electronic structure of carbon and enhance the interactions between the N-doped biochar with the organic pollutant [14,48]. Additionally, N species serve as a Lewis basic sites, so they will promote the adsorption of pollutants through Lewis acid–base interactions and can undergo electrostatic attraction with the negatively charged OFGs of pollutants (Figure 1) [14]. Oppositely, B species can provide Lewis acid sites [49] that can be linked to Lewis base sites on the pollutant for Lewis acid–base interactions. F doping can promote biochar adsorption efficiency by H-bonding with -NH and -OH groups and/or other H-donors of the pollutants.

Table 1. An overview of biochar preparation and performance in adsorption of organic pollutants.

Biochar Precursor and Synthesis	Performance	Removal Mechanism	Ref
• Peanut shells • Pyrolysis: 700 °C • N, S co-doping: Thiourea + biochar, pyrolysis: 350 °C, 1 h	• [DEP] = 20 mg L^{-1}, [Biochar] = 1 g L^{-1}, pH = 7 • Q_e of 3.60 ± 0.20 mg g^{-1} and k_2 of 0.04 ± 0.05 g mg^{-1} min^{-1} in 4 h	• Oxidized S and pyridinic N were crucial in the adsorption process • Removal efficiency remained ≥80% after 5 cycles (used biochar was washed with methanol)	[47]
• Hickory sawdust + boric acid • Pyrolysis: 700 °C, 2 h	• [SMX] = 50 mg L^{-1}, [Biochar] = 0.5 g L^{-1}, pH = 5 • Q_e of 94.76 mg g^{-1} in 240 min	• Enhanced porosity and SSA by boric acid activation promoted better adsorption capacity • Adsorption capacity and SSA were in well agreement (R^2 = 0.9091), indicating that adsorption followed the pore-filling process • Adsorption capacity decrease from 94.76 to 64.62 mg g^{-1} after 5 cycles (NaOH treatment of used catalyst after every cycle)	[50]
• Tapioca peels + S doping • Pyrolysis: 800 °C, 3 h, N_2 atmosphere	• [RhB] = 25 mg L^{-1}, [Biochar] = 2 g L^{-1}, pH = 8 • 92.6% removed in 120 min	• Biochar had homogeneous surface interactions with RhB via monolayer adsorption system • Adsorption was controlled by H-bonding, surface interaction, and electrostatic attraction • Adsorption efficiency decreased with each cycle (NaOH treatment of used catalyst after every cycle)	[51]
• Livistona chinensis • Pyrolysis: 500 °C, 4 h, N_2 atmosphere	• [MG] = 150 mg L^{-1}, [Biochar] = 1 g L^{-1}, pH = 7 ± 0.5 • 99.7% removed in 24 h	• Adsorption was best described by Langmuir isotherm model (R^2 = 0.97)	[52]
• Grapefruit peel • Pyrolysis: 400 °C, 2 h • Modification with $FeSO_4$ and $FeCl_3$	• [BPA] = 150 mg L^{-1}, [Biochar] = 1 g L^{-1}, pH = 7 ± 0.5 • Saturated adsorption capacity 9.7098 mg g^{-1} after 150 min	• Chemical adsorption is rate control step in adsorption with non-uniform adsorbent and evenly distributed energy of surface adsorption • Adsorption mechanism was controlled by a variety of forces (i.e., π-π EDA interaction, H-bond, etc.)	[53]
• Sawdust + Zn and Fe loading • Pyrolysis: 600 °C, 2 h, N_2 atmosphere	• [TET] = 150 mg L^{-1}, [Biochar] = 1 g L^{-1}, pH = 6	• Adsorption process was controlled by chemisorption • H-bond between OH of TET and OFGs biochar along with the π-π EDA interactions promote fast sorption • After desorption (using NaOH treatment), the adsorption decrease from 91.6% to 89% after 3 cycles	[45]
• Rice straw • Pyrolysis: 700 °C, 2 h • H_3PO_4 treatment	• [TC] = 120 mg L^{-1}, [Biochar] = 2/3 g L^{-1} • Qe of 166.3 mg g^{-1} in 192 h	• Π-π EDA interactions and H-bonding are ascribed as primary sorption mechanisms	[54]
• Pomelo peels • Pyrolysis: 450 °C, 15 min • Chitosan treatment for chitosan–biochar hydrogel beads	• [CIP] = 50 mg L^{-1}, [Biochar] = 0.1 g L^{-1}, pH = 3–10 • Sorption capacity of 36.72 mg g^{-1}	• Adsorption efficiency remained similar at pH 3–10 but significantly decreases at higher pH • Adsorption mechanisms encompassed π-π EDA interaction, H-bonding, and hydrophobic interaction • OFGs groups such as -OH and -COOH on biochar make it more hydrophilic for hydrophobic interaction with CIP • F and N heteroaromatic ring of CIP allow it to act as π electron acceptor	[46]

3.2. H_2O_2 Activation

Chemical oxidants such as H_2O_2, PS, and O_3 are capable of treating organic effluents. However, due to their relatively mild oxidative potentials, catalytic activation using biochar

to generate reactive species is desirable. The activation process follows an electron transfer regime between the activator (biochar) and the oxidant, and these activation mechanisms are influenced by the properties of the peroxide (O-O) bond (i.e., bond distance and dissociation energy). Among the common oxidants, H_2O_2, with a redox potential of 1.76 V vs. NHE [55], is highly preferable in water treatment because its decomposition products are only oxygen and hydrogen, which is considered environmentally friendly to water treatment [56]. The H_2O_2 structure encompasses an O-O bond distance of 1.460 Å with a dissociation energy of 377 kJ/mol. In a biochar/H_2O_2 system, the electron transfer process from biochar to H_2O_2 molecules induces the breakage of the O-O or O-H bond for subsequent ROS formations. Table 2 overviews the performance and mechanism of H_2O_2 activation by biochar catalysts. The H_2O_2 activation process can yield various ROS, including hydroxyl radicals ($^{\bullet}OH$) and superoxide radicals ($^{\bullet}O_2^{-}$) [57], which will consequently attack the organic molecules. The fission of the H_2O_2 bonds by biochar activation is taken place by the surface active sites of biochar with electron-donating capacities, amongst which electron-rich OFGs are most effective in H_2O_2 activation. For example, Sun et al. [58] found that after using biogas residue-derived biochar to treat some organic pollutants in the H_2O_2 system, the contents of C-OH, C-O, and C=O in the biochar were reduced compared with those before the catalytic cycle, indicating the contribution of these species as the catalytic active sites. In addition, the internal electron transfer from amorphous carbon (sp.^{3}) to graphitic carbon (sp.^{2}) is fruitful in H_2O_2 activation as the later carbon configuration can subsequently transfer electrons to H_2O_2 [59]. PFRs, with strong electron-donating capacities, provide excellent H_2O_2 activation sites. The activation of H_2O_2 by PFRs takes place by a single electron process from PFRs for the consequent O-O bond breakage and $^{\bullet}OH$ formation [59]. For instance, Huang et al. [60] found that $K_2Cr_2O_7$ addition to the biochar/H_2O_2/DMPO-OH system significantly quenched $^{\bullet}OH$ content and lowered the PFRs concentration due to $K_2Cr_2O_7$ cutting off the electron transfer from PFRs to H_2O_2. N doping is efficient in modulating electronic properties of the carbon lattice of biochar, allowing it to have better electron-donating capacity and hence better H_2O_2 activation performance. Previously, Luo et al. [59] found that pyridinic N decreased from 24.10 at % to 15.86 at % and pyridinic N decreased from 32.24 at % to 22.25 at % after using sludge-derived biochar in H_2O_2 activation for CIP removal, indicating the importance of these N species in sharing electrons with neighboring C atoms compared to other N species (i.e., pyrrolic N and graphitic N). Similarly, Sun et al. [58] found that the graphitic and pyridinic N content of biogas residue-derived biochar decreased after the reaction, stipulating that graphitic and pyridinic N were more operative than pyrrolic N in activating H_2O_2.

Other than the formation of reactive radicals, H_2O_2 activation by biochar can promote nonradical pathways, in which the produced species experience less oxidative potential than the radical pathways. A nonradical pathway is more resistant toward being affected by conventional scavengers, inorganic ions, and pH changes [61,62]. During this pathway, the breakage of the O-O bond is not a prerequisite. According to reports, the nonradical pathways in biochar/H_2O_2 include the production of singlet oxygen ($^1O_2$) and surface-bound $^{\bullet}OH$. For example, it was found that the activation of H_2O_2 by low temperature (300 °C) derived biochar was dominated by $^{\bullet}OH$ generation, whereas high pyrolysis temperature (800 °C) derived biochar catalytic reaction was dominated by $^1O_2$ generation [58]. $^1O_2$ is obtainable via the hydrolysis of $^{\bullet}O_2^{-}$ [63]. Another study found that surface-bound $^{\bullet}OH$ was the key ROS for the degradation of MNZ in the H_2O_2 system [64]. Although the surface-bound radicals are more resistant toward different water matrixes, for free radicals, the organic pollutants have higher probability for productive reaction with ROS as they exist in the bulk of the solution, allowing reactions on and nearby the catalysts' surface. However, for the organic molecules to react with surface-bound radicals, the interaction between the oxidant and substrate is confined to take place on the catalyst surface.

Table 2. An overview of biochar preparation and performance in H_2O_2 activation for organic pollutants removal.

Biochar Precursor and Synthesis	Performance	Removal Mechanism	Ref
• Maize straw + Fe-impregnation • Pyrolysis: 700 °C, 2 h, N_2 atmosphere	• [SMX] = 10 μM, [Biochar] = 1 g L^{-1}, [H_2O_2] = 3 mM, pH = 5 • 100% removed in 2 h	• C-OH activates H_2O_2 to produce $^{\bullet}$OH, $HO_2^{\bullet}$, and alkyl radicals to degrade SMX	[65]
• Sewage sludge • Pyrolysis: 500 °C, 4 h, N_2 atmosphere • Acid (HNO_3) treatment	• [CIP] = 10 mg L^{-1}, [Biochar] = 1 g L^{-1}, [H_2O_2] = 10 mM, pH = 7.4 • 93% removed in 24 h	• Single-electron transfer from biochar PFRs to H_2O_2 induced $^{\bullet}$OH generation • Consumption of $sp.^3$ and $sp.^2$ carbons indicated and electron transfer regime from amorphous carbon to graphitic carbon, as the latter serves as a reactive site • C=O, pyridinic N, and pyridinic N were active sites for the activation by electron transfer to H_2O_2	[59]
• Wheat straws • Pyrolysis: 700 °C, 2 h, N_2 atmosphere	• [SMT] = 13.7 μM, [Biochar] = 1 g L^{-1}, [H_2O_2] = 3 mM, pH = 5 • 100% removed in 2 h	• SSA and porosity were crucial in SMT adsorption and catalytic $^{\bullet}$OH generation • Biochar surface acidity was negatively correlated with catalytic activation, whereas surface basicity was positively correlated with catalytic activation • Excessive SMT adsorption prior to activation hindered H_2O_2 activation	[66]
• Biogas residue + $KHCO_3$ activation • Pyrolysis: 800 °C, 3.5 h, N_2 atmosphere • Acid (HCl) washing	• [Benzene] = 10 μM, [Biochar] = 1 g L^{-1}, [H_2O_2] = 3 mM, pH = 5	• OFGs, C=C, pyridinic N, and graphitic N allowed electron transfer for $^{\bullet}$OH, $^{\bullet}O_2^{-}$, and $^1O_2$ formation • $^1O_2$ generation dominated the catalytic reaction	[58]
• Sewage sludge • Pyrolysis: 600 °C, 30 min • Pyrolysis + kaolin: 1100 °C, 30 min, N_2 atmosphere	• [CIP] = 10 mg L^{-1}, [Biochar] = 0.2 g L^{-1}, [H_2O_2] = 10 mM, pH = 4 • <30% removed after 1 h of adsorption and 80% removed after 20 min from H_2O_2 addition	• Large SSA and inorganic groups enhance CIP adsorption • $\cdot O_2^{-}$ is formed by reactions of $^{\bullet}$OH and H_2O_2	[67]
• Pig manure • Pyrolysis: 500 °C, 2 h, N_2 atmosphere	• [TC] = 30 mg L^{-1}, [Biochar] = 0.5 g L^{-1}, [H_2O_2] = 5 mM, pH = 7.4 • 100% removed in 240 min	• Electron transfer pathway from PFRs to H_2O_2 was responsible for $^{\bullet}$OH formation • TC adsorption can block the active site and minimize reactions between PFRs and H_2O_2, lowering activation performance • Removal efficiency decreased from 100% to 74.5% in 4th run	[60]
• Sugarcane residues + Fe impregnation • Pyrolysis: 600 °C, 4 h	• [OG] = 0.1 g L^{-1}, [Biochar] = 0.5 g L^{-1}, [H_2O_2] = 0.075 g L^{-1}, pH = 5.5 • 99.7% removed within 2 h	• $HO_2^{\bullet}$ and $^{\bullet}$OH are a function of H_2O_2 concentration • Catalytic degradation preferred lower pH due to the higher oxidative potential of $HO_2^{\bullet}$ and $^{\bullet}$OH, slower decomposition of H_2O_2 to H_2O and O_2, and formation of inner-sphere complexes of Fe oxides and OG	[68]
• Sugarcane bagasse + steel pickling waste liquor • Pyrolysis: 400 °C, 2 h, N_2 atmosphere	• [MNZ] = 40 mg L^{-1}, [Biochar] = 0.3 g L^{-1}, [H_2O_2] = 5 mM, pH = 5.61 • 100% removed within 2 h	• Surface-bounded $^{\bullet}$OH were the major ROS responsible for degradation	[64]

3.3. O_3 Activation

O_3 is widely used for wastewater disinfection due to its high redox potential (E° = 2.08 V). Ozone may also directly oxidize organic pollutants with the targeting of C=C or N=N bonds [69]. However, direct ozonation is limited by selective interactions with organic molecules under acidic conditions. Additionally, O_3 direct reaction with some organics such as saturated carboxylic acids and inactivated aromatics is slow, making it difficult to achieve complete mineralization [70]. Nonetheless, enhanced ozonation can be achieved by catalytic activation for escalated ROS generation and faster O_3 decomposition. Table 3 provides an overview on the performance and mechanism of biochar in O_3 activation. Apparently, OFGs of biochar are efficacious in O_3 activation by the adsorption of dissolved O_3 and its catalytic activation. For example, Zhang et al. [71] used sludge-derived biochar for catalytic ozonation to treat phenol. The elemental analysis of biochar before and after catalytic

activation illustrated the disappearance of carbonyl groups and emergence of carboxyl group after the reaction. From these results and upon studying the effects of catalytic parameters, it can be concluded that the electron-rich C=O active sites are of paramount importance in adsorbing dissolved O_3, then initiating its rapid decomposition to produce $^\bullet O_2^-$ that will cause the oxidation of C=O groups to O-C=O. Moreover, chromene-like and pyrone-like OFGs can reactively react with O_3 through the Criegee mechanism to form H_2O_2, which then reacts with the surface-active sites of carbonaceous catalyst or O_3 to yield $^\bullet OH$ [72]. In addition, O_3 adsorption and decomposition to form $^\bullet OH$ prefers the Lewis acid sites on the biochar surface [73,74]. Therefore, it is expected that B doping can endow Lewis acid sites on the biochar surface [75] and promote the O_3 activation performance. Meanwhile, Li et al. [76] found that the high density of C=C groups supplied efficient delocalized π-electrons. These electrons will react with H_2O to form hydroxide (OH^-) and H_3O^+ that will correspondingly yield $HO_2^\bullet$, $^\bullet O_2^-$, and $^\bullet OH$ after reaction with O_3.

Table 3. An overview of biochar preparation and performance in O_3 activation for organic pollutants removal.

Biochar Precursor and Synthesis	Performance	Removal Mechanism	Ref
• Coking wastewater treatment sludge • Pyrolysis: 700 °C, 2 h, N_2 atmosphere	• [Phenol] = 0.2 g L^{-1}, [Biochar] = 1 g L^{-1}, [O_3] = 14 ± 1 mg L^{-1}, 1.0 L min^{-1} • 95.4% removed in 30 min	• C-O and C=O served as active sites for ozone catalytic decomposition • C=O adsorbed dissolved O_3 and initiated its rapid decomposition for $\cdot O_2^-$ generation • C=O was oxidized into O-C=O after reaction • Presence of HCO_3^- promoted $^\bullet OH$ and $HCO_3^\bullet$ formation, reacting with O_3 for $^\bullet O_2^-$ generation • Removal efficiency decreased from 95.4% to 59.3% in 4th cycle	[71]
• Activated petroleum waste sludge • Pyrolysis: 850 °C, 1 h, N_2 atmosphere	• [Benzoic acid] = 100 mg L^{-1}, [Biochar] = 1 g L^{-1}, [O_3] = 20 mg min^{-1}, pH = 3.8–10.0 • ≥95% removed in 30 min	• Functional C groups, Si-O groups, metallic oxides of Zn, Al, Fe, and Mg are expected as the active sites • Reaction was suggested to be mediated by $^\bullet OH$ • Excessive adsorption under acidic conditions leads to competition with ozonation process • Removal efficiency fell to 79.1% in 5th cycle	[77]
• Peanut shell • Pyrolysis: 600 °C, 4 h, N_2 atmosphere	• [KET] = 2 mg L^{-1}, [Biochar] = 500 mg L^{-1}, [O_3] = 0.5 L min^{-1}, pH = 6 ± 0.1 • 99.9% removed in 3 min	• O_3 direct or indirect attack on C=O, C=C, and -OH on biochar initiated radical chain reactions • Delocalized π-electrons react with H_2O to form hydroxide OH^- and H_3O^+ that will yield HO_2, $^\bullet O_2^-$, and $^\bullet OH$ after reaction with O_3 • $^1O_2$, $^\bullet O_2^-$, and $^\bullet OH$ were the main species responsible for degradation • Removal efficiency decreased to 94.8% in 5th cycle	[76]

Similar to H_2O_2 activation, O_3 activation by biochar can bring rise to nonradical oxidative pathways, such as surface-confined $^\bullet OH$, $^1O_2$, surface-O_3 complex, surface adsorbed atomic oxygen ($^*O_{ad}$), and direct electron transfer pathway [74,78]. $^*O_{ad}$ species, with 2.43 V oxidation potential, are formed when O_3 molecules are adsorbed on defective edges (i.e., zigzag, vacancies, and armchair edges). Chemisorbed O_3 molecules on these sites are prone to dissociation into $^*O_{ad}$ and free peroxide species. The $^*O_{ad}$ can attack the adsorbed organic pollutants by the nonradical pathway or react with H_2O and generate surface-adsorbed $^\bullet OH$ [72]. Electron transfer can occur from the organic molecules to the O_3 with the biochar acting as an electron tunnel. Specific active sites such as graphitic N in biochar can provide an electron mobility region for the successful flow of electrons from the pollutant to O_3 to achieve the nonradical degradation of these organics (Figure 2) [79]. However, these nonradical pathways are rarely reported in a biochar/O_3 system compared to other carbonaceous allotropes (e.g., CNTs, hollow sphere carbon) due to limited research on the mechanism of biochar as an O_3 activator.
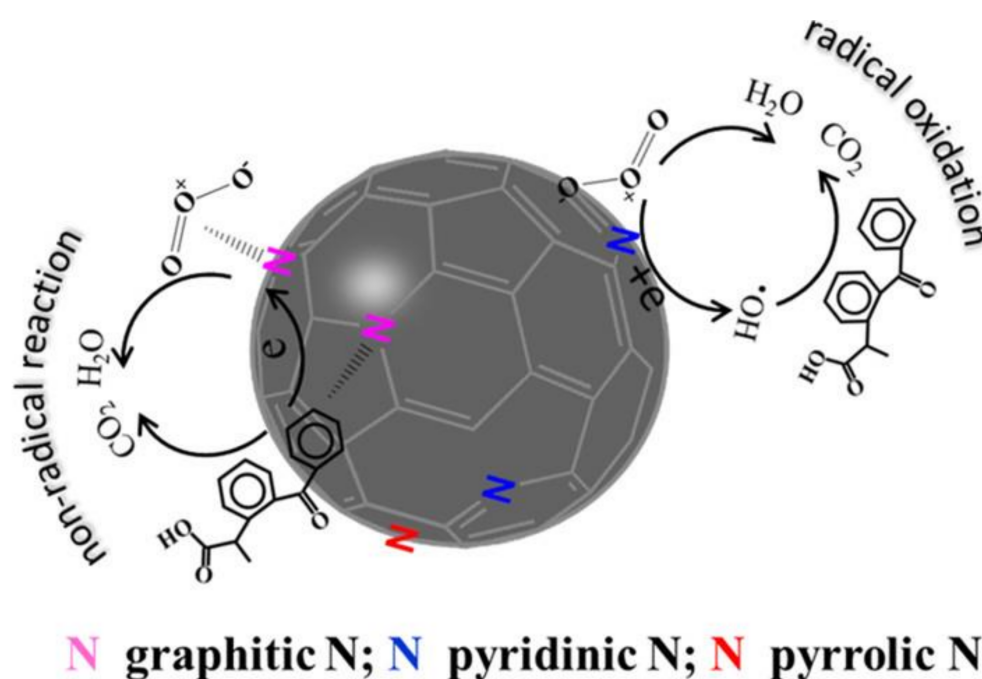
N graphitic N; N pyridinic N; N pyrrolic N

Figure 2. Mechanism of KET degradation by N-doped carbon. Reprinted with permission from Sun et al. [79]. Copyright 2019 American Chemical Society.

3.4. PS Activation

Recently, sulfate radical ($SO_4^{\bullet-}$)-based AOPs (SR-AOPs) have gained attention for organic pollutant degradation. Generally, $SO_4^{\bullet-}$ can be achieved through the activation of PS such as peroxymonosulfate (PMS) and peroxydisulfate (PDS). Table 4 provides an overview on biochar performance in PS activation to remove organic pollutants. In the radical pathway, PS can generate $SO_4^{\bullet-}$ through undergoing peroxide bond cleavage. $SO_4^{\bullet-}$ (+2.6 V vs. NHE) possesses comparable standard redox potential with $^{\bullet}OH$ (+2.80V vs. NHE), which makes it a suitable substitute for the conventional use of $^{\bullet}OH$ in AOPs [80]. It should be noted that $^{\bullet}OH$ may be present in SR-AOPs due to the reaction of $SO_4^{\bullet-}$ with water to form $^{\bullet}OH$ radicals [80,81]. On the other hand, PS can also be activated through a nonradical pathway, in which free moving radicals are not involved in organics mineralization. In the biochar/PS system, a nonradical pathway can proceed through surface-bound radicals [40,82], surface-confined complexes [83], electron mediation mechanism, and $^1O_2$ generation. Similar to H_2O_2 activation, surface-bound radicals such as $SO_4^{\bullet-}$ and $^{\bullet}OH$ can oxidize organic pollutants in close proximity to the biochar. Surface-bound radicals are favored by improved PS adsorption on biochar. For instance, Ding et al. [82] reported that the PMS adsorption by biochar (derived from a phytoremediation plant) on the graphitic N site facilitates the formation of adsorbed radicals through receiving electron from the surrounding carbon of the biochar, while the adsorbed pollutant will act as an electron donor and undergo oxidation. Meanwhile, biochar can be used as an electron mediator to generate a direct electron transfer pathway through the transfer of electrons between PS and the pollutant. Typically, a higher extent of graphitization favors the electron mediator pathway due to the enhanced pollutant adsorption (by π-π interaction) and increased surface conductivity of the biochar [29,39,84]. Lastly, $^1O_2$ generation can be achieved by the reaction of PS with the ketonic groups of biochar [85–87]. Furthermore, there are also reports suggesting the involvement of $O_2^{\bullet-}$ as an intermediate for $^1O_2$ generation [88,89].

Generally, biochar with adequately graphitized C, high defective degree, better active sites (ketonic O and/or heteroatom dopant), and large SSA are favorable for PS activation. Defects in sp.^{2} carbon lattice can induce charge localization, thereby facilitating PS adsorption for activation to generate various ROS for pollutant degradation [33,90,91]. The enrichment of π-π* transitions in the aromatic rings of the biochar provides it with the ability to generate free radicals. For instance, Zhu et al. [40] used sawdust-derived biochar (0.5 g L^{-1}) for CA (0.1 mM) removal under PDS (10 mM) activation. The degradation rate after 60 min was 97.8%. Upon scavenging studies, it is concluded that the π-π* transitions activate PDS to form $SO_4^{\bullet-}$ and correspondingly generate $^{\bullet}OH$. The contribution of π-π* transition was reflected in the reduction of its content from 5.68% to 4.46% after catalytic usage. The conjugated π-aromatic structure can be used as electron-donating moieties [41] that enhance the catalytic performance via the electron donation process to PS for O-O bond splitting. However, this effect is less commonly reported due to the presence of other active sites on biochar that experience stronger electron donation capacity, such as electron-rich ketonic groups, which will compete with the aromatic conjugated system.

The active sites of biochar can be modulated by using different biomass and heteroatom doping. For instance, Meng et al. [13] found that biochar derived from cellulose-rich biomass favors PS activation due to its high ketonic group content and larger SSA when compared with lignin-rich biomass. Furthermore, heteroatom doping also shows promising results in PS activation. For instance, the doping of N atoms into biochar has been shown to improve PS activation by increasing the charge density (graphitic N) of surrounding carbon and also improving the electron-donating properties of the biochar (pyridinic and pyrrolic N) [15,29,92], while doping B species can introduce a Lewis acid group, which can facilitate PS adsorption and activation [49]. The multi-heteroatom doping of biochar utilizes possible synergistic interactions between different heteroatoms to alter the charge and spin density of C in biochar, which may be beneficial for PS activation. For instance, the synergistic interaction of N (graphitic N) and S (thiophenic S) in biochar has been shown to be able to redistribute the charge density of the C lattice in biochar, which will improve the electron-donating properties of biochar and facilitate PS activation [93–95].

Apparently, the role of PFR in activating PS is inconclusive. There are studies suggesting that PFR can effectively activate PS [96,97]. For instance, Zhang et al. [97] found that biochar prepared by thermal treatment at 500 °C has an antibiotics removal rate equivalent to that of PMS activation with biochar prepared at 900 °C (active sites: defective sites), due to the presence of carbon-centered PFRs in lower synthesis temperature that can activate PMS for radical generation. On the other hand, Li et al. [33] found that PFRs do not contribute significantly to activating PDS for ofloxacin degradation. Hence, more studies are needed to ascertain the role of PFR in PS activation. Despite its potential, the uses of PFR may be limited because PFRs are easily consumed, which will result in poor reusability in activating PS.

Table 4. An overview of biochar preparation and performance in PS activation for organic pollutants removal.

Biochar Precursor and Synthesis	Performance	Removal Mechanism	Ref
• Food waste digestate • Pyrolysis: 800 °C, 2 h, N$_2$ atmosphere	• [X-3B] = 1 g L^{-1}, [Biochar] = 0.5 g L^{-1}, [PDS] = 1.5 mM, pH = 3.78 • 85.72% removed in 30 min	• sp.^{2} carbon served to produce radicals by PDS activation in an electron-accepting process • Graphitic and pyridinic N facilitated ROS generation • C=O contributed to $^1O_2$ formation • Removal efficiency decreased from 85.72% to 32.53% at 30 min in 2nd cycle	[98]
• Peanut shells • Pyrolysis: 900 °C, 2 h, N$_2$ atmosphere	• [SMT] = 40 μM, [Biochar] = 0.2 g L^{-1}, [PMS] = 1 mM, pH = 6 • 98.3% removed in 120 min	• Sieving to small-sized biochar (0–75 μm) enhanced PDS activation due to more graphitic and aromatic carbon, COOH content, and higher SSA • COOH groups promoted $SO_4^{\bullet-}$ and $^{\bullet}OH$ formation • Biochar mediated electron transfer from SMT to PDS • Electron-rich active sites transfer electrons to PDS for $SO_4^{\bullet-}$, $^{\bullet}OH$, $^1O_2$, and $^{\bullet}O_2^-$ generation	[99]

Table 4. *Cont.*

Biochar Precursor and Synthesis	Performance	Removal Mechanism	Ref
• Spent tea leave • Pre-oxidation: 250 °C, 0.5 h, air environment • Pyrolysis: 500 °C, 1 h, N_2 atmosphere	• [CTC] = 50 mg L^{-1}, [Biochar] = 0.1 g L^{-1}, [PDS] = 1 g L^{-1}, pH = 6.0 • 97.4% removed in 90 min	• Pre-adsorption was beneficial to the subsequent catalytic degradation • Delocalized π-electrons and Fe facilitated $SO_4^{\bullet-}$, $^\bullet OH$, and $^1O_2$ generation	[100]
• Dairy manure • Anaerobic digestion: 37 °C, 35 days • Pyrolysis: 800 °C, 2 h, N_2 atmosphere	• [SMX] = 15 mg L^{-1}, [Biochar] = 1 g L^{-1}, [PMS] = 2.5 mM, pH = 5.56 • 90.2% removed in 60 min	• Defects were positively correlated with degradation potential (R^2 = 0.92) • Electron-rich C=O promoted $^\bullet O_2^-$ and $^1O_2$ generation • Graphitic N accelerated electron transfer from carbon to O_2 for $^1O_2$ formation • Pyridine N was not an active site • Graphitic structure facilitated electron transfer between SMX and PMS • Removal efficiency decreased from 90.2% to 62.5% in 5th cycle	[101]
• Straw • Pyrolysis: 700 °C, 2 h, N_2 atmosphere • N doping: Thiourea + biochar, pyrolysis: 800 °C, 2 h, N_2 atmosphere	• [TC] = 20 mg L^{-1}, [Biochar] = 200 mg L^{-1}, [PDS] = 2 mM, pH = 7 • 97% removed in 60 min and 100% in 120 min	• Reaction mainly relied on nonradical electron transfer between TC and PDS due to enhanced graphitization degree • Radicals had no effect on TC degradation • Removal efficiency decreased from 100% to 55% in 3rd cycle	[102]
• Rice husk • Pyrolysis: 850 °C, 1 h	• [SMX] = 500 μg L^{-1}, [Biochar] = 100 mg L^{-1}, [PDS] = 500 mg L^{-1} • 96% removed in 120 min	• Reaction controlled by either electron transfer/$^1O_2$ control surface-bound radicals	[103]
• Wheat straw + B doping • Pyrolysis: 900 °C, 2 h, N_2 atmosphere • KOH activation: 600 °C, 2 h, N_2 atmosphere • Acid (HCl) washing	• [SMX] = 20 mg L^{-1}, [Biochar] = 0.1 g L^{-1}, [PDS] = 1 mM, pH = 6.3 • 94% removed in 120 min	• B species acted as Lewis acid sites enhancing PDS adsorption • Defects and sp.^{2}-conjugated π-system facilitated electron transfer • B substitution in carbon matrix enhanced catalyst stability due to active sites reversible transformation during catalytic activation • Removal efficiency decreased from 92% to 90% in 5th cycle	[49]
• Wood shavings + N and S co-doping • Pyrolysis: 800 °C, 2 h	• [MB] = 8 mg L^{-1}, [Biochar] = 0.2 g L^{-1}, [PMS] = 0.4 g L^{-1}, pH = 3–4 • >95% removed in 30 min	• Synergy between S and N moieties altered surrounding electron density • $^\bullet OH$, $SO_4^{\bullet-}$, and $^1O_2$ participated in the catalytic reaction • Removal rate decreased gradually from 0.202 min^{-1} to 0.019 min^{-1} in 4th cycle	[95]
• Corncob + N doping • Pyrolysis: 700 °C, 2 h, N_2 atmosphere	• [SDZ] = 10 μM, [Biochar] = 3 g L^{-1}, [PDS] = 1 mM, pH = 7 • 96.2% removed in 10 min	• Pyridinic and pyrrolic N at edge sites disturbed electron density to create active sites • Graphitic N was not well correlated with catalytic activity • PDS was reduced at electron-rich N while SDZ was oxidized around adjacent electron-deficient C • Reaction was dominated by an electron transfer regime that was unaffected by inorganic anions except NOM • Removal efficiency decreased from 96.5% to 83.0% after 3 cycles	[15]
• Wetland plants (reed) + N doping • Pyrolysis: 900 °C, 90 min, N_2 atmosphere	• [OG] = 50 mg L^{-1}, [Biochar] = 0.2 g L^{-1}, [PDS] = 2 mM, pH = 9.5 ± 0.8 • 100% removed in 60 min	• Quaternary N induces asymmetric spin density and low electron density to adjacent carbons, facilitating the chemical bonding with negatively charged O atoms of the O-O bond in PDS for free radicals formations • Large SSA and $\pi-\pi$ interactions between OG aromatic rings graphitic carbon structure enhanced adsorption • Catalytic activity was governed by nonradical pathway of surface-activated PDS complexes and $^1O_2$ • Removal efficiency decreased from 98.3% to 45.0 ± 2.0% after 5 runs	[92]

Table 4. *Cont.*

| Biochar Precursor and Synthesis	Performance	Removal Mechanism	Ref
• Spirulina residue + N doping • Pyrolysis: 900 °C, 90 min, N$_2$ atmosphere • Acid (HCl) washing	• [SMX] = 20 mg L^{-1}, [Biochar] = 0.5 g L^{-1}, [PDS] = 6 mM • 100% removed in 45 min	• Biochar provided electron-mediating medium between SMX and PDS for nonradical degradation • N doping caused a redistribution of charge densities in graphitic carbons where PDS will then bond with positively charged O atoms adjacent to N dopants to enhance activation performance • Surface-activated metastable PDS/carbon complex participated in reaction • Removal efficiency decreased from 100% to 42.51% after 3 cycles	[29]

3.5. Photocatalysis

Photocatalytic degradation of organic pollutants has been extensity studied in the last few decades. Typically, metals oxides such as TiO$_2$, ZnO, and BiVO$_4$ have been commonly used as a photocatalyst for environmental application. During photocatalytic reactions, the absorption of electromagnetic radiation by the photocatalyst is crucial to activate the photocatalyst and produce ROS, which can be used to degrade organic pollutants. The energy of the absorbed light irradiation must be greater or equal to the bandgap energy (Eg) of that photocatalyst in order to excite the electrons from the conduction band (CB) to the valence band (VB) [104]. When the excited electrons (e$_{cb}^-$) migrate to CB, positive holes (h$_{vb}^+$) will be formed in VB. Then, the electron/hole pair will migrate to the surface of the semiconductor to react with the adsorbed substrates. Generally, e$_{cb}^-$ will react with the electron acceptors adsorbed on the catalyst surface to reduce it, whereas h$_{vb}^+$ will react with electron donors on the catalyst surface to oxidize it [105,106]. Dissolved O$_2$ and OH$^-$ ions in water can interact as electron acceptors and electron donors, respectively. The e$_{cb}^-$ can reduce O$_2$ to generate $^\bullet$O$_2^-$ whereas h$_{vb}^+$ can react with the OH$^-$ to generate $^\bullet$OH. Nonetheless, $^\bullet$O$_2^-$ can only be generated when the CB potential is more negative than the reduction potential of O$_2$/$^\bullet$O$_2^-$ (-0.33 eV). As for $^\bullet$OH formation, the VB potential edge of the photocatalyst must be sufficiently positive to oxidize hydroxide ions or adsorbed H$_2$O to form $^\bullet$OH (OH$^-$/$^\bullet$OH: +2.38 eV, H$_2$O/$^\bullet$OH: +2.72 eV) [107–109].

Recently, biochar has been found to have a semiconductor-like structure and serves as an active carbonaceous photocatalyst. Table 5 provides the performance and mechanism of biochar as a photocatalyst to remove organic pollutants. When used as a photocatalyst, biochar OFGs (i.e., C=O, C-OH) can behave as photosensitizers, as they allow the excited electron to be transferred to the adsorbed electron acceptor (e.g., O$_2$) for ROS generation [110]. Among OFGs, quinone moieties are capable of generating ^{1}O$_2$. The quinone-like moieties are first excited under light irradiation to singlet states. The excited states will undergo an intersystem crossing to yield excited triplet states quinone moieties through additional photonic excitation. These species further react with dissolved oxygen to produce ^{1}O$_2$ by an energy transfer regime [111]. The light photons can be absorbed by the defective sites that serve as VB, leading to the activation of biochar and the excitation of electrons. Due to the excellent conductivity of biochar, the excited electron will migrate to OFGs that are serving as biochar CB. The e$_{cb}^-$ of OFGs with effective redox potentials will react with adsorbed O$_2$ to generate $^\bullet$O$_2^-$ and h$_{vb}^+$ on defects will directly attack the adsorbed pollutants (Figure 3) [112]. Hence, the highly graphitized structure is important in photocatalysis as it allows better electron transfer from the biochar to the absorbed species to form ROS.

Table 5. An overview of biochar preparation and performance as photocatalyst activation for organic pollutants removal.

Biochar Precursor and Synthesis	Performance	Removal Mechanism	Ref
• Pine needles • Pyrolysis: 500 °C, 2 h	• [DEP] = 20 mg L^{-1}, [Biochar] = 0.2 g L^{-1}, pH = 7, 100 W Hg lamp (350–450 nm) • 72.3% removed within 120 min	• $^\bullet$OH was dominate species contributing to 76.7–82.8% DEP removal • UV irradiation excited quinone-like moieties to singlet states and then rapidly went through an intersystem crossing to yield excited triplet states that further reacted with dissolved oxygen by energy transfer to form $^1O_2$ • PFRs can mediate electron transfer to O_2 for $^\bullet$OH formation • Electron transfer from VB to CB and electron–hole pairs formation allows electrons transfer to redox-active functional groups defects to form relatively stable PFRs	[111]
• Wheat straw • Pyrolysis: 500 °C, 2 h	• [DEP] = 20 mg L^{-1}, [Biochar] = 0.2 g L^{-1}, pH = 7, 100 W Hg lamp (350–450 nm) • 60.9% removed within 120 min	• $^\bullet$OH was dominate species contributing to 76.7–82.8% DEP removal • UV irradiation excited quinone-like moieties to singlet states and then rapidly went through an intersystem crossing to yield excited triplet states that further reacted with dissolved oxygen by energy transfer to form $^1O_2$ • PFRs can mediate electron transfer to O_2 for $^\bullet$OH formation • Electron transfer from VB to CB and electron–hole pairs formation allows electrons transfer to redox-active functional groups defects to form relatively stable PFRs	[111]
• Poplar woodchips • Pyrolysis: 300 °C, 3 h • Ball milling	• [EFA] = 20 mg L^{-1}, [Biochar] = 0.2 g L^{-1}, pH = 7, 500 W Xe lamp (UV cut-off filter), pH = 6.8 • 80.2% removed after 1.5 h under dark and 2.5 h under illumination	• More amounts of phenolic structures and defects on ball-milled biochar aided in $\cdot O_2{}^-$ generation • OFGs, particularly O-C=O, was important in ROS generation • OFGs acted as CB and defects acted as VB, forming a semiconductor-like structure • Excited electrons after light exposure react with O_2 to form $O_2{}^-$ • h$^+$ on the defects with strong oxidative and $O_2{}^-$ will attack EFA	[112]
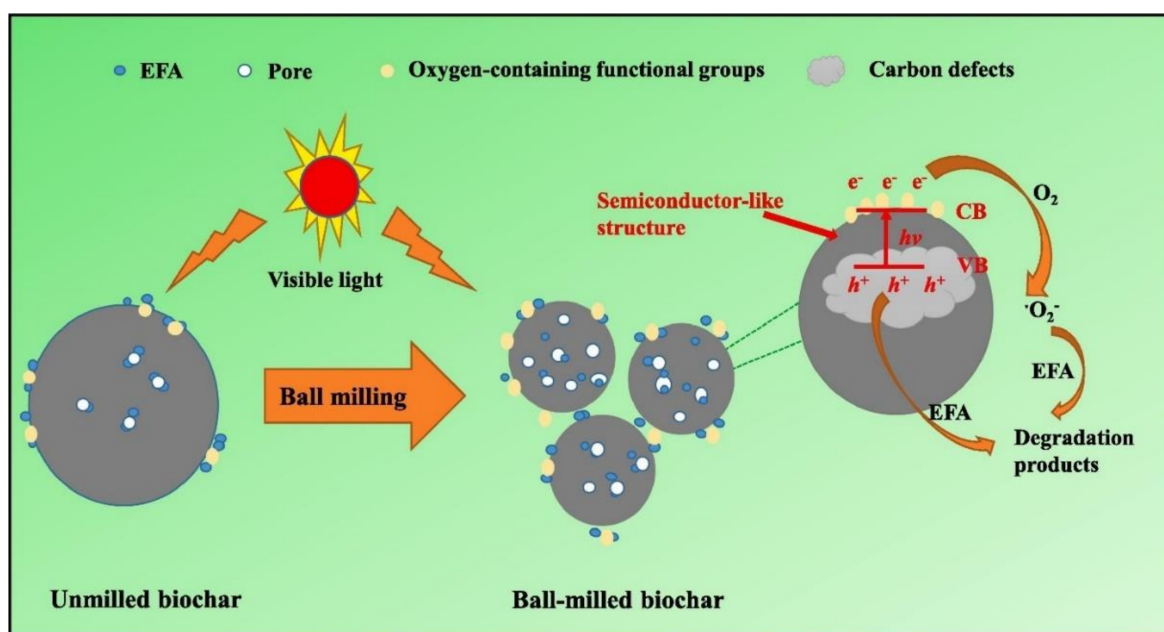
Figure 3. Mechanism of photocatalytic degradation of EFA by ball-milled biochar. Reprinted from Xiao et al. [112]. Copyright 2019, with permission from Elsevier.

Regardless, there are limited studies on the potential of biochar as a photocatalyst and even less reports on the effect of heteroatomic doping on the photocatalytic activity of biochar. Since S doping can alleviate the HOMO–LUMO transitions and induce spin charges in the carbon framework [113], S doping into biochar is expected to have a positive effect on the biochar photocatalytic performance under visible light. In addition, because N is easily doped into the carbon structure, it allows the facile tuning of carbonaceous local electronic properties due to different electronegativity with carbon atoms [114]. It can have a fruitful effect on the photonic activation of biochar.

4. Comparison

The performance of biochar in treating organic pollutants varies significantly through different applications. Herein, the use of biochar in adsorption, Fenton reactions, O_3 activation, PS activation, and photocatalysis is evaluated with respect to their performance, organics removal mechanism, tolerance to water matrixes, reusability, and economics. It is noteworthy that a direct comparison between different applications is not feasible due to their different mechanisms in the remediation of organic pollutants.

4.1. Performance

The prime variable to be considered when comparing the different applications of biochar is the performance of each application in terms of organics removal. Organics decontamination rates via biochar through different applications is difficult to be compared and evaluated due to the diverse factors affecting the treatment speed, viz. organic pollutant nature, water matrix properties, and biochar active sites. With respect to the properties of organic pollutants, adsorption is the most advantageous in removing oxidation-resistant organic pollutants. On the other hand, AOPs can mineralize recalcitrant pollutants or decompose pollutant molecules into less recalcitrant products, which can be then treated by conventional biodegradation techniques. When using biochar as an adsorbent, the adsorption process will continue until the sorption capacity of the biochar is achieved. For the oxidant systems (O_3, H_2O_2, PS), the oxidative reaction will extend until (i) the catalytic active sites of the biochar are fully deactivated, or (ii) all the oxidant/pollutant molecules are consumed. In the photocatalytic reactions, the reasons for ceasing the catalytic oxidation include the deactivation of biochar active sites, the occupation of the active sites of organic molecules, and the discontinuity of light irradiation. Generally, in all cases, controlling the operational parameters is important to ensure effective treatment. In adsorption, the insufficient sorption capacity of biochar and surface deactivation of biochar can be solved by increasing the load of biochar catalyst. This will provide extra active sites for adsorption and catalytic reactions. Ensuring that the biochar composition is free of toxic components (i.e., polyaromatic hydrocarbons, PFRs, CN^- compounds [22]) is crucial to prevent secondary pollution. In photocatalysis, although increasing the biochar loading is beneficial, increasing the biochar loading beyond the optimal point may have a negative impact. An excessive increase in photocatalyst loading can cause light scattering and decrease light penetration into the active sites on the catalyst surface, leading to a less efficient catalytic reaction [115,116]. In addition, for the oxidant systems, increasing the oxidant concentrations can improve the catalytic reaction significantly. For instance, increasing the PMS dosage from 2.0 to 16.0 mM resulted in an increase in the degradation efficiency of 1,4-dioxane from 22.7% to 88.8% [91]. Nonetheless, the opposite trends have also been reported. For example, increasing the H_2O_2 dosage to an excessive point will decrease the CIP degradation efficiency, which was ascribed to the depletion of the biochar surface active sites by the excessive H_2O_2 content [59]. However, the low resistance of the biochar surface toward excessive H_2O_2 dosage can be ascribed to the high amorphous structure (sp.^{3}-carbon = 25.06%) of the used biochar. Since amorphous C is less stable (compared to graphitized C structure), amorphous C atoms can be considered as vulnerable sites for undesired cannibalistic reactions on the biochar surface during oxidative reactions. Other drawbacks of increasing the oxidant content include higher cost and undesirable

competition between the oxidant molecules and organic pollutants over biochar surface-active sites [117].

All application of photocatalysis, PS, H_2O_2, and O_3 activation must undergo the adsorption of organics before the degradation reaction occurs. However, for a single adsorption system, the goal is to increase the adsorption capacity of the biochar. As for other applications, moderate adsorption is usually desired to avoid an excessive accumulation of organic molecules and adverse occupation of biochar surface active sites, thereby hindering the degradation reaction. During the photocatalytic reaction, excessive adsorption of pollutants on the surface of biochar will prevent the efficient absorption of light irradiation and quench the catalytic reaction. For the oxidant system, immoderately adsorbed organics molecules will compete with the oxidant molecules over the biochar surface active sites, thereby preventing the activation of these oxidants, because the adsorption of the oxidant may be a prerequisite of its activation [33]. For instance, Huang et al. [66] found that increasing the adsorption time of SMT on wheat straw-derived biochar prior to H_2O_2 addition into the system had an inhibitory effect on H_2O_2 activation. Similarly, PMS activation was found to be hampered by the addition of organics pollutants to the biochar systems [118]. Therefore, for oxidant systems and photocatalytic applications of biochar, optimized adsorption is best to be below 50% of the total removal to allow the degradation and catalytic activation of biochar to occur along with the synergistic effect of adsorption removal.

4.2. Removal Mechanism

4.2.1. Pollutant–Biochar Interactions

Organic pollutants can be decontaminated by interacting with the biochar through (i) physical interactions, (ii) chemical interactions, and (iii) redox reactions. Physisorption of organic pollutants is the physical interactions between the biochar surface and the organic pollutants, whilst the chemical interactions are when the organic pollutant is chemically bounded (grafted) into the biochar. Physisorption is promoted by the electrostatic forces and intermolecular attraction between the biochar and the organic pollutant that is controlled by Van deer Waals weak forces by utilizing the biochar surface charge. Physisorption by electrostatic attraction is highly influenced by the surface change of biochar and pollutants. Chemisorption, on the contrary, occurs when stronger chemical bonds such as H-bonds and coordination bond, and covalent bonds are formed between the pollutant and the active sites of biochar [119,120]. In addition, the enthalpy of physisorption (20–40 kJ/mol) is less than that of chemisorption (200–400 kJ/mol) [120,121]. Both types of adsorption can co-exist in one system. Redox reactions in biochar/pollutant systems (i.e., AOPs) involve performing oxidation and reduction reactions that will mineralize, degrade, or alter the chemical composition of the organic pollutant rather than just adsorb it. This can be achieved through nonradical interaction in the presence of oxidant.

4.2.2. Biochar Active Sites Involvement and Produced ROS

The contribution of biochar active sites and the way they serve as active sites varies by applications. Likewise, the produced reactive species (during AOPs) are also different. From the overview in Section 3, Table 6 summarizes the contribution and function of biochar active sites in each application. During the adsorption processes, as no degradation reaction is taking place, PFRs and electron-donating defects are not reported as adsorption sites. To compare oxidants systems, it is predicted that O_3, H_2O_2, and PS activation all share the same active sites involvement due to their similar activation process of O-O bond breakage. Nonetheless, PS activation makes full use of biochar active sites, whilst H_2O_2 activation and O_3 activation have no aromatic structure contribution. In addition, H_2O_2 activation does not utilize defective sites. The dissimilarity between the PS activation against H_2O_2 activation and O_3 activation in terms of the contribution of aromatic structure and defective sites can be ascribed to the variance between O-O properties of each oxidant. Indeed, there is less reports on H_2O_2 activation and O_3 activation compared to PS activation. Therefore,

there is a high chance of all biochar active sites contributing for all oxidant systems. Hence, it is suggested to conduct more research on the biochar/oxidant systems, focusing on the activation mechanism. As for photocatalysis, all considered active sites contribute to the activation expect for the aromatic structure.

　　　With regard to the active species generated during AOPs, all AOPS share the ability to generate ROS, such as $^{\bullet}OH$, $^{\bullet}O_2^-$, and $^1O_2$. However, due to limited reports, it is difficult to compare the efficiency of each system in terms of the formation of active species. Biochar acting as an electron tunnel between oxidant pollutant has only reported for O_3 [79] and PS activation [99]. For nonradical pathways, all oxidant systems have surface-confined active species. For instance, nonradical PS activation can yield a larger variety of surface-confined species, encompassing surface-bound $SO_4^{\bullet-}$, surface-bound $^{\bullet}OH$, and surface-activated PS complexes. Secondly, O_3 activation can provide the biochar surface with surface-bound $^{\bullet}OH$, surface-bound O_3 complexes, and $^*O_{ad}$. Lastly, H_2O_2 activation can only generate surface-bound $^{\bullet}OH$. Generally, free ROS has a stronger redox potential compared with the surface-bound species due to the surface-confinement effect [122]. However, the redox potential of surface-bound $SO_4^{\bullet-}$, surface-bound $^{\bullet}OH$, and surface-activated PS complexes is currently unknown, whereas that of $^*O_{ad}$ is 2.43 V [72]. As for other distinctions between the systems, the formation of $SO_4^{\bullet-}$ has a high oxidative potential (2.5–3.1 V), and selectivity toward organics with electron-rich groups, unsaturated bonds, and aromatic π-electrons [22] is constrained to PS activation. Additionally, electron tunneling in biochar/H_2O_2 has not been reported, which may be ascribed to its lower redox potential compared to PS and O_3. Moreover, the electron transfer process is expected to be more easily realized in PDS systems than in PMS and H_2O_2 systems as the former has a higher redox potential (2.01 V_{NHE} for PDS vs. 1.82 V_{NHE} for PMS vs. 1.776 V_{NHE} for H_2O_2 [123]), making it more prone to serve as an electron acceptor. As for photocatalysis, it is the sole application that can produce reductive h_{VB}^+, which can directly degrade pollutants. Figure 4 summarizes the generated active species of each application of biochar.
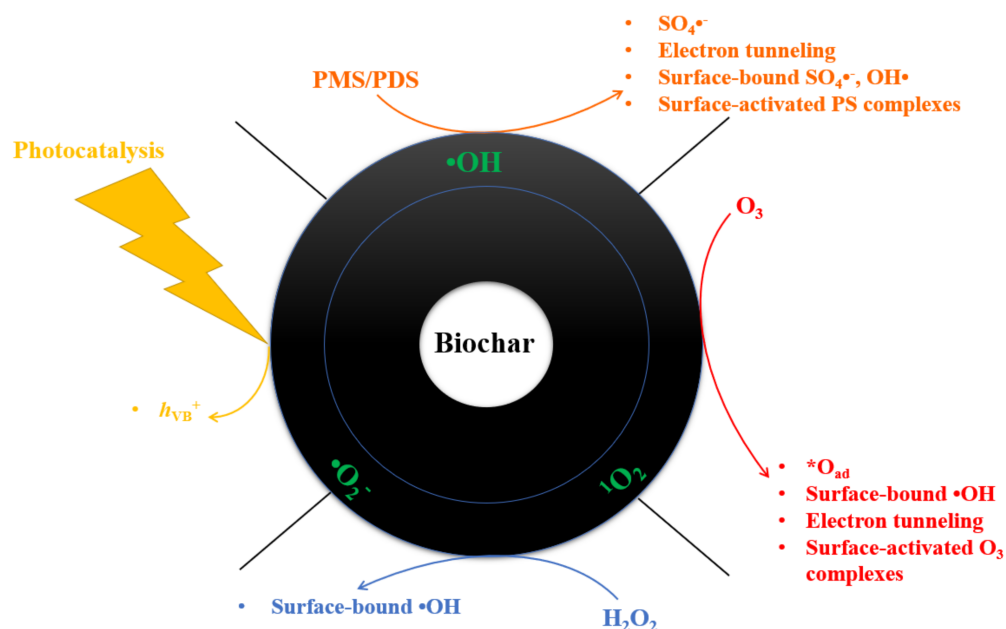

Figure 4. Produced active species in biochar during different AOPs systems.

Table 6. Comparison on the function/s of biochar active sites in different organic pollutants treatment applications.

Active Site	Adsorption	H_2O_2 Activation	O_3 Activation	PS Activation	Photocatalysis
• OFGs	• Induce H-bonding, ion exchange, π-π interactions, and Coulombic attraction • -OH and -COOH increase hydrophilicity to promote hydrophobic interactions with hydrophobic organics	• Electron-rich OFGs are most effective in H_2O_2 activation	• Electron-rich C=O groups aid in adsorbing dissolved O_3 and initiating rapid decomposition for $^\bullet O_2^-$ generation • Chromene-like and pyrone-like OFGs can reactively react with O_3 to form H_2O_2 to yield $^\bullet OH$	• Electron-rich OFGs such as C=O are effective in PS activation • Acid OFGs (COOH) inhibit PS activation	• OFGs behave as photosensitizers to transfer excited electron to adsorbed electron acceptor for ROS generation • Quinone moieties excitation cycle can generate $^1O_2$
• Carbon hybridization status	• Graphitized structure allows π-π EDA interactions adsorption	• Internal electron transfer from sp.^{3} carbon to sp.^{2} carbon then to H_2O_2 for activation	• C=C groups supply delocalized π-electrons to react with H_2O to form OH^- and H_3O^+ that will yield $HO_2^\bullet$, $^\bullet O_2^-$, and $^\bullet OH$ after reacting with O_3	• Graphitized structure improves pollutant adsorption and conductivity (facilitate electron mediator mechanism)	• Graphitized structure allows better electron transfer from biochar to adsorbed electron acceptors
• Defects	–	–	• Provide adsorption sites for O_3 • Chemisorbed O_3 molecules on defects can dissociate into $^*O_{ad}$ and free peroxide species	• Defective sites can serve as active site for PS activation	• Defective sites can absorb light by serving as VB, causing the activation biochar and excitation of electrons • h_{vb}^+ on defects can directly attack the adsorbed pollutants
• Aromatic structure	• Conjugated π-aromatic structure can act as electron donating moieties to promote π-π EDA interactions with organics pollutants having electron-accepting moieties	–	–	• Aromatic structure can act as electron-donating moieties for PS activation (but lower reactivity than other functional groups)	–
• PFRs	–	• Single electron transfer process from PFRs for the consequent O-O bond breakage and $^\bullet OH$ formation	–	• Can activate PS (not conclusive)	• PFRs can trigger $^\bullet OH$ generation
• Heteroatoms	• F and N behave as H-acceptors for H-bonding • N doping can alter the electronic structure of biochar and enhance electronic interactions with pollutant • N species as Lewis basic sites can promote adsorption by Lewis acid–base interactions • N species can undergo electrostatic attraction with negatively charged OFGs of pollutants • B species can provide Lewis acid sites that can link with pollutants Lewis acid sites for Lewis acid–base interactions • F doping can promote adsorption by H-bonding with H donors of pollutant	• N doping can modulate electronic properties of carbon lattice for better electron donating capacity and better H_2O_2 activation	• B doping can introduce Lewis acid sites for O_3 adsorption and decomposition for $^\bullet OH$ formation • Graphitic N can provide electron mobility for the flow of electrons from the pollutant to O_3 for nonradical pathway	• Heteroatoms modulate C charge density to facilitate PS activation • Heteroatom can act as active sites (pyridinic N, pyrrolic N, thiophenic S, B-OH)	• S doping can ease HOMO–LUMO transitions and induce spin charges in the carbon framework • N doping tunes biochar local electronic properties due to different electronegativity with C atoms

4.3. Tolerance to pH Changes

The most important factor affecting water treatment is the pH of the reaction solution. The pH of the reaction mixture determines the surface charge of the biochar and the existing speciation of the pollutants. Generally, the point of zero charge (PZC) of biochar is between 7.1 and 10.5 [124]. As such, when the biochar surroundings' pH is equal to the PZC of that catalyst, the catalyst surface will be neutral with a zero net electric charge. At any pH below the PZC, the catalyst surface will be positively charged (protonated) and its surface will be negatively charged (deprotonated) at pH values above the PZC. Furthermore, strong alkaline conditions can accelerate the dissociation of the acidic functional groups of biochar [112]. Hence, a strong acidic condition is expected to promote the decomposition of alkaline surface sites of biochar. Certain biochar active sites are not influenced by pH. For instance, the carbon hybridization status and aromatic structure are not influenced by changes in pH. The effect of pH on the performance of PFRs in initiating redox reactions remains uncertain. Yu et al. [125] found that oxygen-centered PFRs on N-doped char were the main active site for PMS activation to remove endocrine-disrupting compounds. The removal performance over a wide pH range of 4–10 was almost unaffected. This may indirectly point out that the ability of PFR to perform redox reactions is not affected by changes in pH.

During the adsorption process, a higher pH can promote the dissociation of the -OH groups of pollutant and affect the H-bonding adsorption [126]. On the other hand, adsorption mechanism such as π-π EDA interactions are not affected by pH changes, as it only requires the successful interactions between biochar as an electron donor and pollutant as electron acceptor, which is not affected by the surrounding pH [126]. As mentioned earlier, all AOPs require adsorption prior to catalytic reactions to provide productive interactions between the biochar surface active sites and the pollutant molecules. Consequently, the effect of pH on the initial adsorption of pollutants has a similar effect on the efficiency of O_3 activation [76], PMS activation [127], PDS activation [102], and H_2O_2 activation [59]. As for reactive species formation, $^{\bullet}OH$ prefers intermediate to alkaline conditions, as it promotes a higher conversion rate of OH^- to $^{\bullet}OH$. Furthermore, $SO_4^{\bullet-}$ functions well at a wide pH range of 2.0–8.0 [128]. Most efficiently, $^1O_2$ is capable of adapting to pH changes [22]. In addition, under strong alkali conditions, PMS mainly exists as SO_5^{2-}, which prevents the sufficient $SO_4^{\bullet-}$ generation [129].

4.4. Stability and Reusability

The reusability of biochar is highly important as it improves time and cost efficiency. During the adsorption process, the biochar usually reaches its adsorption capacity, and the active adsorption sites are fully occupied. Therefore, a regeneration process is essential after saturation. Nevertheless, the regeneration of biochar via the desorption process is relatively facile, and it can be done through thermal or chemical regeneration. Meanwhile, during the application in a highly oxidizing environment (i.e., AOPs), the biochar-active sites may undergo chemical oxidation. This is because the generated ROS and radicals may not be able to distinguish between the organic pollutant and the biochar surface, as both are carbon, causing the cannibalistic attacks on the biochar surface. As a result, without careful control, biochar can only be used for several consecutive cycles without the need of regeneration processes. For instance, when using sludge-derived biochar as an O_3 activator, the activation performance is reduced from 95.4% to 59.3% in the fourth cycle. Upon studying the chemical properties of the catalyst surface, it was noticed that the active carbonyl group (C=O) completely disappeared from the biochar and was replaced by the carboxyl group (O-C=O), indicating that the surface was oxidized during the activation process [71]. Likewise, Oh et al. [30] found that in a biochar/PMS system, the graphitic N would be undergo reconstruction to form pyridinic N [30]. In addition, for photocatalytic reactions, the biochar surface active sites are endangered by both cannibalistic reaction by radicals and light-induced decomposition. During the photocatalytic oxidation, extensive light irradiation, especially UV light, can induce the decomposition of the surface functional

groups of biochar [111], showing the importance of using visible light irradiation. Generally, the active sites can be restored via thermal treatment [29]. Additionally, since the major changes of the biochar surface after the AOPs cycle are the oxidation of the active sites, the chemical regeneration by the reducing agents can be efficient in restoring the deactivated sites. For instance, Hou et al. [130] found that treating the spent carbonaceous catalysts with sodium borohydride (NaBH$_4$, strong reducing agent) can remove O-C=O groups and increase basic sites in restoring some activity; however, it caused the undesirable loss of N species.

For all AOPs, synthesizing biochar with high aromaticity can promote stability. An aromatic structure with a well-packed carbon structure and bond electron resonance can provide tolerance toward undesirable oxidative and cannibalistic reactions on the biochar surface (unlike alkyl moieties), which can enhance the durability of the active sites. For separation, metallic doping is often used to bear the biochar with magnetic properties to facilitate separation. Nevertheless, metal leaching can cause secondary pollution. To overcome these drawbacks, a biochar/polymer composite can be fabricated for undemanding separation. This is a win–win strategy, as the biochar can enhance the mechanical, thermal, and electrical properties of the polymer [131,132], and the polymer film will ease the reusability and catalyst stability. Amongst polymers, organics decontamination using floating (low-density) polymer-based materials (e.g., linear low-density polyethylene (LLDPE)) is highly desirable as no stirring is required, separation of catalyst is facile, and the floating of the catalyst allows excellent utilization of light irradiation (in the case of photocatalysis). In addition, a biochar/polymer composite has a longer lifespan of e/h pairs and thus allows better photocatalytic activity [133]. In addition, optimizing the reaction condition to ensure the maximized mineralization of organic pollutants will reduce the content of adsorbed by-products on the biochar surface and maintain the concentration of active sites.

4.5. Economics

Economically, all applications share the synthesis expenditure of biochar (capital cost) in which the total production cost is estimated to be approximately $0.91 per kg, with 40% yield along with the production of useful amounts of bio-oil [52]. As per application, operational cost varies significantly. The adsorption process is the cheapest compared to AOPs because it does not require oxidant or external energy sources (e.g., light, sonication). The desorption cost, on the other hand, is dependent on the desorption technique. In addition, since adsorption is only transferring the pollutants from one phase to another, secondary treatment is required to mineralize these organics. Therefore, the total cost of treatment of organics via adsorption includes and is influenced by the cost of the secondary treatment method. As for photocatalysis, the major cost factor is the irradiation source. Conventional light sources (i.e., mercury lamps, fluorescence lamps) are relatively expensive and produce noticeable heat while irradiating, causing an additional loss of electrical cost. Solar irradiation has been often reported as an efficient light source for photocatalytic reactions to overcome this drawback [134–136]. However, atmospheric changes need to be considered. Light-emitting diodes (LED) are getting attention as light sources for photocatalytic reactions [137–139] due to their low cost, high light intensity with less electrical power, and lower heat generation compared with fluorescence and mercury lamps [140,141].

As for the biochar/oxidant systems, the catalytic reaction cost is a function of the price of the oxidant. Between the oxidants, O$_3$ is the most expensive oxidant, as its generation requires the use of an electrical discharge over pure oxygen or air. This process consumes significant amounts of energy and capital cost; therefore, it is considered economically undesirable [69]. Optimized O$_3$ production over a range of only 10 wt% to 12 wt% is estimated to cost $2.00/kg [142]. In addition, the actual O$_3$ dosage in the catalytic reactions is experimentally measured by the difference between the inlet O$_3$ volume and the outflow [143], which indicates that the measurable amounts of O$_3$ can be lost without being completely used, causing an inefficient utilization of the oxidant, hence leading to higher

cost. PS and H_2O_2 rarely or will not encounter this problem. As for the other oxidants, PMS (Oxone), PDS ($Na_2S_2O_8$), and H_2O_2 (30%) are priced at \$26.4/kg, \$50.8/kg, and \$192/L, respectively (Sigma Aldrich).

5. Conclusions and Future Prospects

Thus far, biochar, as a carbonaceous material with various active sites, has been successfully utilized in the decontamination of organic pollutants from water by different applications. Among the numerous applications of biochar in wastewater treatment, adsorption, H_2O_2 activation, O_3 activation, PS activation, and photocatalysis hold the superlative potential in the treatment of organic pollutants. These applications were compared with respect to performance, mechanism of removal with emphasis on pollutant–biochar interactions and biochar active sites' involvement, tolerance to changes in water pH, stability of biochar after consecutive cycles of pollutant treatment, and economic factors. Each application has its own advantages and limitations. Adsorption is superior in terms of simplicity of operational procedures, ability to remove oxidation-resistant pollutants, and cost-wise. AOPs utilize more active sites of biochar and are able to mineralize organics pollutants or form less resistant organic by-products, so they can be treated by conventional methods. All AOPs have their own advantages. For instance, PS activation is effective in utilizing all of the biochar active sites along with having a monopoly on the capability to produce $SO_4^{\bullet-}$. H_2O_2 is a safe oxidant with nonharmful decomposition products (hydrogen and oxygen). O_3 is a strong oxidant with various activation pathways. Photocatalysis does not require the use of any oxidant. Nonetheless, limitations are present in each application. (i) The low durability of biochar active sites during AOPs is repeatedly reported. In addition, (ii) the performance of pristine biochar for environmental remediation of organic pollutants is often slow with low efficiency. (iii) The cost of light source during photocatalytic reactions is a drawback. (iv) Adsorption is unable to mineralize or degrade organic pollutants. (v) Biochar–pollutant and biochar–oxidant interactions are highly influenced by water pH changes, hindering its application in real wastewater. To enhance biochar performance in environmental remediation, several suggestions can be made:

i.   The fabrication of robust biochar with high graphitization and aromaticity degree can prevent poor durability. In addition, compositing with polymers can protect the active site of biochar from cannibalistic reactions and can also simplify the separation of the catalyst.

ii.   Heteroatom (i.e., N, S, B, F, P) doping is often found to have a fruitful effect on the performance of biochar in environmental remediation. However, co-doping and triple-doping are rarely reported. Hence, more studies are needed on multi-doped biochar, with systematic investigations on the interactions between the multi-dopants within the biochar structure and its effect on the biochar performance. Moreover, as heteroatomic doping of biochar can be achieved by in situ and post-treatment methods, a comparison between the two techniques is needed to determine the most efficient method.

iii.   For photocatalytic applications, LED lamps can be used instead of conventional light sources to avoid an additional cost of electricity and better utilization of energy.

iv.   Synergistic removal by adsorption with other AOPs methods may provide constructive results. Nonetheless, the optimization of adsorption contribution is crucial to avoid undesirable competition over biochar active sites and hinder removal performance.

v.   Specific tailoring of biochar active sites that are unlikely to be affected with pH changes and/or can produce species that are resistant to changing pH (i.e., non-radical pathways) can endow the biochar with better performance over different water matrixes.

tualization, M.F.G. and W.-D.O.; Resources, Y.-C.H., J.-W.L. and W.-D.O.; Supervision, S.-C.L. and W.-D.O.; funding acquisition, Y.-C.H., J.-W.L. and W.-D.O. All authors have read and agreed to the published version of the manuscript.

Data Availability Statement: Not applicable.

Conflicts of Interest: The authors declare no conflict of interest.

Abbreviations

$^*O_{ad}$, surface-adsorbed atomic oxygen; $^1O_2$, singlet oxygen; ACT, acetaminophen; AOPs, advanced oxidation processes; BPA, bisphenol A; CA, clofibric acid; CB, conduction band; CIP, ciprofloxacin; CTC, chlortetracycline; DEP, diethyl phthalate; EDA, electron donor–acceptor; EFA, enrofloxacin; Eg, bandgap; H_2O_2, hydrogen peroxide; KET, ketoprofen; LED, light-emitting diodes; MB, methylene blue; MG, malachite green; MDZ, metronidazole; $^\bullet O_2^-$, superoxide radical; O_3, ozone; OG, orange G; OFGs, oxygen functional groups; $^\bullet OH$, hydroxyl radical, OH^-, hydroxyl ion; PDS, peroxydisulfate; PFRs, persistent free radicals; PMS, peroxymonosulfate; PS, persulfate, RhB, rhodamine B; ROS, reactive oxygen species; SDZ, sulfadiazine; SMT, sulfamethazine; SMX, sulfamethoxazole; $SO_4^{\bullet-}$, sulfate radical; SR-AOPs, sulfate radical-based AOPs; SSA, specific surface area; TC, tetracycline; TET, tetracycline; VB, valence band; X-3B, reactive brilliant red X-3B.

References

1. Anh, H.Q.; Le, T.P.Q.; Da Le, N.; Lu, X.X.; Duong, T.T.; Garnier, J.; Rochelle-Newall, E.; Zhang, S.; Oh, N.H.; Oeurng, C.; et al. Antibiotics in surface water of East and Southeast Asian countries: A focused review on contamination status, pollution sources, potential risks, and future perspectives. *Sci. Total Environ.* **2021**, *764*, 142865. [CrossRef] [PubMed]
2. Briffa, J.; Sinagra, E.; Blundell, R. Heavy metal pollution in the environment and their toxicological effects on humans. *Heliyon* **2020**, *6*, e04691. [CrossRef] [PubMed]
3. Choong, Z.-Y.; Lin, K.-Y.A.; Lisak, G.; Lim, T.-T.; Oh, W.-D. Multi-heteroatom-doped carbocatalyst as peroxymonosulfate and peroxydisulfate activator for water purification: A critical review. *J. Hazard. Mater.* **2021**, *426*, 128077. [CrossRef] [PubMed]
4. Offiong, N.-A.O.; Inam, E.J.; Etuk, H.S.; Ebong, G.A.; Inyangudoh, A.I.; Addison, F. Trace Metal Levels and Nutrient Characteristics of Crude Oil-Contaminated Soil Amended with Biochar–Humus Sediment Slurry. *Pollutants* **2021**, *1*, 119–126. [CrossRef]
5. Offiong, N.A.O.; Inam, E.J.; Etuk, H.S.; Essien, J.P.; Ofon, U.A.; Una, C.C. Biochar and humus sediment mixture attenuates crude oil-derived PAHs in a simulated tropical ultisol. *SN Appl. Sci.* **2020**, *2*, 1930. [CrossRef]
6. Bharagava, R.N.; Saxena, G.; Mulla, S.I.; Patel, D.K. Characterization and Identification of Recalcitrant Organic Pollutants (ROPs) in Tannery Wastewater and Its Phytotoxicity Evaluation for Environmental Safety. *Arch. Environ. Contam. Toxicol.* **2017**, *75*, 259–272. [CrossRef]
7. van Duin, D.; Paterson, D.L. Multidrug-Resistant Bacteria in the Community: Trends and Lessons Learned. *Infect. Dis. Clin. N. Am.* **2016**, *30*, 377–390. [CrossRef]
8. Rathi, B.S.; Kumar, P.S. Application of adsorption process for effective removal of emerging contaminants from water and wastewater. *Environ. Pollut.* **2021**, *280*, 116995. [CrossRef]
9. Fonseca Couto, C.; Lange, L.C.; Santos Amaral, M.C. A critical review on membrane separation processes applied to remove pharmaceutically active compounds from water and wastewater. *J. Water Process Eng.* **2018**, *26*, 156–175. [CrossRef]
10. Kanakaraju, D.; Glass, B.D.; Oelgemöller, M. Advanced oxidation process-mediated removal of pharmaceuticals from water: A review. *J. Environ. Manag.* **2018**, *219*, 189–207. [CrossRef]
11. Suliman, W.; Harsh, J.B.; Abu-Lail, N.I.; Fortuna, A.M.; Dallmeyer, I.; Garcia-Perez, M. Influence of feedstock source and pyrolysis temperature on biochar bulk and surface properties. *Biomass Bioenergy* **2016**, *84*, 37–48. [CrossRef]
12. Chandra, S.; Bhattacharya, J. Influence of temperature and duration of pyrolysis on the property heterogeneity of rice straw biochar and optimization of pyrolysis conditions for its application in soils. *J. Clean. Prod.* **2019**, *215*, 1123–1139. [CrossRef]
13. Meng, H.; Nie, C.; Li, W.; Duan, X.; Lai, B.; Ao, Z.; Wang, S.; An, T. Insight into the effect of lignocellulosic biomass source on the performance of biochar as persulfate activator for aqueous organic pollutants remediation: Epicarp and mesocarp of citrus peels as examples. *J. Hazard. Mater.* **2020**, *399*, 123043. [CrossRef] [PubMed]
14. Li, Y.; Xing, B.; Wang, X.; Wang, K.; Zhu, L.; Wang, S. Nitrogen-Doped Hierarchical Porous Biochar Derived from Corn Stalks for Phenol-Enhanced Adsorption. *Energy Fuels* **2019**, *33*, 12459–12468. [CrossRef]

15. Wang, H.; Guo, W.; Liu, B.; Wu, Q.; Luo, H.; Zhao, Q.; Si, Q.; Sseguya, F.; Ren, N. Edge-nitrogenated biochar for efficient peroxydisulfate activation: An electron transfer mechanism. *Water Res.* **2019**, *160*, 405–414. [CrossRef]

16. Do Minh, T.; Song, J.; Deb, A.; Cha, L.; Srivastava, V.; Sillanpää, M. Biochar based catalysts for the abatement of emerging pollutants: A review. *Chem. Eng. J.* **2020**, *394*, 124856. [CrossRef]

17. Liang, L.; Xi, F.; Tan, W.; Meng, X.; Hu, B.; Wang, X. Review of organic and inorganic pollutants removal by biochar and biochar-based composites. *Biochar* **2021**, *3*, 255–281. [CrossRef]

18. Wang, J.; Wang, S. Preparation, modification and environmental application of biochar: A review. *J. Clean. Prod.* **2019**, *227*, 1002–1022. [CrossRef]

19. Zhou, X.; Zhu, Y.; Niu, Q.; Zeng, G.; Lai, C.; Liu, S.; Huang, D.; Qin, L.; Liu, X.; Li, B.; et al. New notion of biochar: A review on the mechanism of biochar applications in advannced oxidation processes. *Chem. Eng. J.* **2021**, *416*, 129027. [CrossRef]

20. Luo, K.; Pang, Y.; Wang, D.; Li, X.; Wang, L.; Lei, M.; Huang, Q.; Yang, Q. A critical review on the application of biochar in environmental pollution remediation: Role of persistent free radicals (PFRs). *J. Environ. Sci.* **2021**, *108*, 201–216. [CrossRef]

21. Dai, Y.; Zhang, N.; Xing, C.; Cui, Q.; Sun, Q. The adsorption, regeneration and engineering applications of biochar for removal organic pollutants: A review. *Chemosphere* **2019**, *223*, 12–27. [CrossRef] [PubMed]

22. Gasim, M.F.; Lim, J.-W.; Low, S.-C.; Lin, K.-Y.A.; Oh, W.-D. Can biochar and hydrochar be used as sustainable catalyst for persulfate activation? *Chemosphere* **2022**, *287*, 132458. [CrossRef] [PubMed]

23. Zhao, Y.; Yuan, X.; Li, X.; Jiang, L.; Wang, H. Burgeoning prospects of biochar and its composite in persulfate-advanced oxidation process. *J. Hazard. Mater.* **2021**, *409*, 124893. [CrossRef] [PubMed]

24. Zhou, C.; Wang, Y. Recent progress in the conversion of biomass wastes into functional materials for value-added applications. *Sci. Technol. Adv. Mater.* **2020**, *21*, 787–804. [CrossRef] [PubMed]

25. Başer, B.; Yousaf, B.; Yetis, U.; Abbas, Q.; Kwon, E.E.; Wang, S.; Bolan, N.S.; Rinklebe, J. Formation of nitrogen functionalities in biochar materials and their role in the mitigation of hazardous emerging organic pollutants from wastewater. *J. Hazard. Mater.* **2021**, *416*, 126131. [CrossRef]

26. Li, D.C.; Jiang, H. The thermochemical conversion of non-lignocellulosic biomass to form biochar: A review on characterizations and mechanism elucidation. *Bioresour. Technol.* **2017**, *246*, 57–68. [CrossRef]

27. Lawal, A.A.; Hassan, M.A.; Zakaria, M.R.; Yusoff, M.Z.M.; Norrrahim, M.N.F.; Mokhtar, M.N.; Shirai, Y. Effect of oil palm biomass cellulosic content on nanopore structure and adsorption capacity of biochar. *Bioresour. Technol.* **2021**, *332*, 125070. [CrossRef]

28. Chen, Y.-d.; Duan, X.; Zhang, C.; Wang, S.; Ren, N.Q.; Ho, S.H. Graphitic biochar catalysts from anaerobic digestion sludge for nonradical degradation of micropollutants and disinfection. *Chem. Eng. J.* **2020**, *384*, 123244. [CrossRef]

29. Ho, S.H.; Chen, Y.-d.; Li, R.; Zhang, C.; Ge, Y.; Cao, G.; Ma, M.; Duan, X.; Wang, S.; Ren, N.-q. N-doped graphitic biochars from C-phycocyanin extracted Spirulina residue for catalytic persulfate activation toward nonradical disinfection and organic oxidation. *Water Res.* **2019**, *159*, 77–86. [CrossRef]

30. Oh, W.D.; Lisak, G.; Webster, R.D.; Liang, Y.N.; Veksha, A.; Giannis, A.; Moo, J.G.S.; Lim, J.W.; Lim, T.T. Insights into the thermolytic transformation of lignocellulosic biomass waste to redox-active carbocatalyst: Durability of surface active sites. *Appl. Catal. B Environ.* **2018**, *233*, 120–129. [CrossRef]

31. Liu, H.; Ye, M.; Dong, X.; Ren, Z.; Long, S.; Lichtfouse, E. Removal of humic substances by the synergistic effect of biochar adsorption and activation of persulfate. *J. Water Process Eng.* **2021**, *44*, 102428. [CrossRef]

32. Zaeni, J.R.J.; Lim, J.W.; Wang, Z.; Ding, D.; Chua, Y.S.; Ng, S.L.; Oh, W.D. In situ nitrogen functionalization of biochar via one-pot synthesis for catalytic peroxymonosulfate activation: Characteristics and performance studies. *Sep. Purif. Technol.* **2020**, *241*, 116702. [CrossRef]

33. Li, H.; Liu, Y.; Jiang, F.; Bai, X.; Li, H.; Lang, D.; Wang, L.; Pan, B. Persulfate adsorption and activation by carbon structure defects provided new insights into ofloxacin degradation by biochar. *Sci. Total Environ.* **2021**, *806*, 150968. [CrossRef] [PubMed]

34. Ruan, X.; Sun, Y.; Du, W.; Tang, Y.; Liu, Q.; Zhang, Z.; Doherty, W.; Frost, R.L.; Qian, G.; Tsang, D.C.W. Formation, characteristics, and applications of environmentally persistent free radicals in biochars: A review. *Bioresour. Technol.* **2019**, *281*, 457–468. [CrossRef] [PubMed]

35. Wijitkosum, S.; Jiwnok, P. Elemental Composition of Biochar Obtained from Agricultural Waste for Soil Amendment and Carbon Sequestration. *Appl. Sci.* **2019**, *9*, 3980. [CrossRef]

36. Kim, D.G.; Ko, S.O. Effects of thermal modification of a biochar on persulfate activation and mechanisms of catalytic degradation of a pharmaceutical. *Chem. Eng. J.* **2020**, *399*, 125377. [CrossRef]

37. Yu, J.; Tang, L.; Pang, Y.; Zeng, G.; Feng, H.; Zou, J.; Wang, J.; Feng, C.; Zhu, X.; Ouyang, X.; et al. Hierarchical porous biochar from shrimp shell for persulfate activation: A two-electron transfer path and key impact factors. *Appl. Catal. B Environ.* **2020**, *260*, 118160. [CrossRef]

38. Yu, J.; Tang, L.; Pang, Y.; Zeng, G.; Wang, J.; Deng, Y.; Liu, Y.; Feng, H.; Chen, S.; Ren, X. Magnetic nitrogen-doped sludge-derived biochar catalysts for persulfate activation: Internal electron transfer mechanism. *Chem. Eng. J.* **2019**, *364*, 146–159. [CrossRef]

39. Ye, S.; Zeng, G.; Tan, X.; Wu, H.; Liang, J.; Song, B.; Tang, N.; Zhang, P.; Yang, Y.; Chen, Q.; et al. Nitrogen-doped biochar fiber with graphitization from Boehmeria nivea for promoted peroxymonosulfate activation and non-radical degradation pathways with enhancing electron transfer. *Appl. Catal. B Environ.* **2020**, *269*, 118850. [CrossRef]

40. Zhu, K.; Wang, X.; Geng, M.; Chen, D.; Lin, H.; Zhang, H. Catalytic oxidation of clofibric acid by peroxydisulfate activated with wood-based biochar: Effect of biochar pyrolysis temperature, performance and mechanism. *Chem. Eng. J.* **2019**, *374*, 1253–1263. [CrossRef]

41. Zhang, Y.; Xu, X.; Cao, L.; Ok, Y.S.; Cao, X. Characterization and quantification of electron donating capacity and its structure dependence in biochar derived from three waste biomasses. *Chemosphere* **2018**, *211*, 1073–1081. [CrossRef] [PubMed]

42. Nageeb, M. Adsorption Technique for the Removal of Organic Pollutants from Water and Wastewater. In *Organic Pollutants—Monitoring, Risk and Treatment*; InTech: London, UK, 2013.

43. Duan, Q.; Li, X.; Wu, Z.; Alsaedi, A.; Hayat, T.; Chen, C.; Li, J. Adsorption of 17β-estradiol from aqueous solutions by a novel hierarchically nitrogen-doped porous carbon. *J. Colloid Interface Sci.* **2019**, *533*, 700–708. [CrossRef] [PubMed]

44. Tong, Y.; McNamara, P.J.; Mayer, B.K. Adsorption of organic micropollutants onto biochar: A review of relevant kinetics, mechanisms and equilibrium. *Environ. Sci. Water Res. Technol.* **2019**, *5*, 821–838. [CrossRef]

45. Zhou, Y.; Liu, X.; Xiang, Y.; Wang, P.; Zhang, J.; Zhang, F.; Wei, J.; Luo, L.; Lei, M.; Tang, L. Modification of biochar derived from sawdust and its application in removal of tetracycline and copper from aqueous solution: Adsorption mechanism and modelling. *Bioresour. Technol.* **2017**, *245*, 266–273. [CrossRef] [PubMed]

46. Afzal, M.Z.; Sun, X.F.; Liu, J.; Song, C.; Wang, S.G.; Javed, A. Enhancement of ciprofloxacin sorption on chitosan/biochar hydrogel beads. *Sci. Total Environ.* **2018**, *639*, 560–569. [CrossRef] [PubMed]

47. Guo, R.; Yan, L.; Rao, P.; Wang, R.; Guo, X. Nitrogen and sulfur co-doped biochar derived from peanut shell with enhanced adsorption capacity for diethyl phthalate. *Environ. Pollut.* **2020**, *258*, 113674. [CrossRef]

48. Wang, X.; Liu, Y.; Zhu, L.; Li, Y.; Wang, K.; Qiu, K.; Tippayawong, N.; Aggarangsi, P.; Reubroycharoen, P.; Wang, S. Biomass derived N-doped biochar as efficient catalyst supports for CO_2 methanation. *J. CO_2 Util.* **2019**, *34*, 733–741. [CrossRef]

49. Liu, B.; Guo, W.; Wang, H.; Si, Q.; Zhao, Q.; Luo, H.; Ren, N. B-doped graphitic porous biochar with enhanced surface affinity and electron transfer for efficient peroxydisulfate activation. *Chem. Eng. J.* **2020**, *396*, 125119. [CrossRef]

50. Zhang, X.; Gang, D.D.; Zhang, J.; Lei, X.; Lian, Q.; Holmes, W.E.; Zappi, M.E.; Yao, H. Insight into the activation mechanisms of biochar by boric acid and its application for the removal of sulfamethoxazole. *J. Hazard. Mater.* **2021**, *424*, 127333. [CrossRef]

51. Vigneshwaran, S.; Sirajudheen, P.; Karthikeyan, P.; Meenakshi, S. Fabrication of sulfur-doped biochar derived from tapioca peel waste with superior adsorption performance for the removal of Malachite green and Rhodamine B dyes. *Surf. Interfaces* **2021**, *23*, 100920. [CrossRef]

52. Giri, B.S.; Sonwani, R.K.; Varjani, S.; Chaurasia, D.; Varadavenkatesan, T.; Chaturvedi, P.; Yadav, S.; Katiyar, V.; Singh, R.S.; Pandey, A. Highly efficient bio-adsorption of Malachite green using Chinese Fan-Palm Biochar (*Livistona chinensis*). *Chemosphere* **2022**, *287*, 132282. [CrossRef] [PubMed]

53. Wang, J.; Zhang, M. Adsorption Characteristics and Mechanism of Bisphenol A by Magnetic Biochar. *Int. J. Environ. Res. Public Health* **2020**, *17*, 1075. [CrossRef] [PubMed]

54. Chen, T.; Luo, L.; Deng, S.; Shi, G.; Zhang, S.; Zhang, Y.; Deng, O.; Wang, L.; Zhang, J.; Wei, L. Sorption of tetracycline on H_3PO_4 modified biochar derived from rice straw and swine manure. *Bioresour. Technol.* **2018**, *267*, 431–437. [CrossRef] [PubMed]

55. Lim, J.; Hoffmann, M.R. Substrate oxidation enhances the electrochemical production of hydrogen peroxide. *Chem. Eng. J.* **2019**, *374*, 958–964. [CrossRef]

56. Li, W.; Bonakdarpour, A.; Gyenge, E.; Wilkinson, D.P. Production of Hydrogen Peroxide for Drinking Water Treatment in a Proton Exchange Membrane Electrolyzer at Near-Neutral pH. *J. Electrochem. Soc.* **2020**, *167*, 044502. [CrossRef]

57. Parrino, F.; Livraghi, S.; Giamello, E.; Ceccato, R.; Palmisano, L. Role of Hydroxyl, Superoxide, and Nitrate Radicals on the Fate of Bromide Ions in Photocatalytic TiO_2 Suspensions. *ACS Catal.* **2020**, *10*, 7922–7931. [CrossRef]

58. Sun, P.; Hua, Y.; Zhao, J.; Wang, C.; Tan, Q.; Shen, G. Insights into the mechanism of hydrogen peroxide activation with biochar produced from anaerobically digested residues at different pyrolysis temperatures for the degradation of BTEXS. *Sci. Total Environ.* **2021**, *788*, 147718. [CrossRef]

59. Luo, K.; Yang, Q.; Pang, Y.; Wang, D.; Li, X.; Lei, M.; Huang, Q. Unveiling the mechanism of biochar-activated hydrogen peroxide on the degradation of ciprofloxacin. *Chem. Eng. J.* **2019**, *374*, 520–530. [CrossRef]

60. Huang, D.; Luo, H.; Zhang, C.; Zeng, G.; Lai, C.; Cheng, M.; Wang, R.; Deng, R.; Xue, W.; Gong, X.; et al. Nonnegligible role of biomass types and its compositions on the formation of persistent free radicals in biochar: Insight into the influences on Fenton-like process. *Chem. Eng. J.* **2019**, *361*, 353–363. [CrossRef]

61. Zhou, X.; Zhao, Q.; Wang, J.; Chen, Z.; Chen, Z. Nonradical oxidation processes in PMS-based heterogeneous catalytic system: Generation, Identification, Oxidation characteristics, Challenges response and Application prospects. *Chem. Eng. J.* **2020**, *410*, 128312. [CrossRef]

62. Chen, F.; Liu, L.-L.; Chen, J.-J.; Li, W.-W.; Chen, Y.-P.; Zhang, Y.-J.; Wu, J.-H.; Mei, S.-C.; Yang, Q.; Yu, H.-Q. Efficient decontamination of organic pollutants under high salinity conditions by a nonradical peroxymonosulfate activation system. *Water Res.* **2020**, *191*, 116799. [CrossRef] [PubMed]

63. Yan, Y.; Yang, Q.; Shang, Q.; Ai, J.; Yang, X.; Wang, D.; Liao, G. Ru doped graphitic carbon nitride mediated peroxymonosulfate activation for diclofenac degradation via singlet oxygen. *Chem. Eng. J.* **2021**, *430*, 133174. [CrossRef]

64. Yi, Y.; Tu, G.; Eric Tsang, P.; Fang, Z. Insight into the influence of pyrolysis temperature on Fenton-like catalytic performance of magnetic biochar. *Chem. Eng. J.* **2020**, *380*, 122518. [CrossRef]

65. Zhang, X.; Sun, P.; Wei, K.; Huang, X.; Zhang, X. Enhanced H2O2 activation and sulfamethoxazole degradation by Fe-impregnated biochar. *Chem. Eng. J.* **2020**, *385*, 123921. [CrossRef]

66. Huang, D.; Wang, Y.; Zhang, C.; Zeng, G.; Lai, C.; Wan, J.; Qin, L.; Zeng, Y. Influence of morphological and chemical features of biochar on hydrogen peroxide activation: Implications on sulfamethazine degradation. *RSC Adv.* **2016**, *6*, 73186–73196. [CrossRef]

67. Li, J.; Pan, L.; Yu, G.; Xie, S.; Li, C.; Lai, D.; Li, Z.; You, F.; Wang, Y. The synthesis of heterogeneous Fenton-like catalyst using sewage sludge biochar and its application for ciprofloxacin degradation. *Sci. Total Environ.* **2019**, *654*, 1284–1292. [CrossRef]

68. Park, J.H.; Wang, J.J.; Xiao, R.; Tafti, N.; DeLaune, R.D.; Seo, D.C. Degradation of Orange G by Fenton-like reaction with Fe-impregnated biochar catalyst. *Bioresour. Technol.* **2018**, *249*, 368–376. [CrossRef]

69. Cuerda-Correa, E.M.; Alexandre-Franco, M.F.; Fernández-González, C. Advanced Oxidation Processes for the Removal of Antibiotics from Water. An Overview. *Water* **2019**, *12*, 102. [CrossRef]

70. Mehrjouei, M.; Müller, S.; Möller, D. A review on photocatalytic ozonation used for the treatment of water and wastewater. *Chem. Eng. J.* **2015**, *263*, 209–219. [CrossRef]

71. Zhang, F.; Wu, K.; Zhou, H.; Hu, Y.; Preis, S.V.; Wu, H.; Wei, C. Ozonation of aqueous phenol catalyzed by biochar produced from sludge obtained in the treatment of coking wastewater. *J. Environ. Manag.* **2018**, *224*, 376–386. [CrossRef]

72. Liu, Y.; Chen, C.; Duan, X.; Wang, S.; Wang, Y. Carbocatalytic ozonation toward advanced water purification. *J. Mater. Chem. A* **2021**, *9*, 18994–19024. [CrossRef]

73. Wang, D.; Xu, H.; Ma, J.; Giannakis, S.; Lu, X.; Chi, H.; Song, S.; Qi, J. Enhanced mineralization of atrazine by surface induced hydroxyl radicals over light-weight granular mixed-quartz sands with ozone. *Water Res.* **2019**, *149*, 136–148. [CrossRef] [PubMed]

74. Tian, S.Q.; Qi, J.Y.; Wang, Y.P.; Liu, Y.L.; Wang, L.; Ma, J. Heterogeneous catalytic ozonation of atrazine with Mn-loaded and Fe-loaded biochar. *Water Res.* **2021**, *193*, 116860. [CrossRef] [PubMed]

75. Wang, Y.; Liu, M.; Zhao, X.; Cao, D.; Guo, T.; Yang, B. Insights into heterogeneous catalysis of peroxymonosulfate activation by boron-doped ordered mesoporous carbon. *Carbon* **2018**, *135*, 238–247. [CrossRef]

76. Li, H.; Liu, S.; Qiu, S.; Sun, L.; Yuan, X.; Xia, D. Catalytic ozonation oxidation of ketoprofen by peanut shell-based biochar: Effects of the pyrolysis temperatures. *Environ. Technol.* **2020**. [CrossRef] [PubMed]

77. Chen, C.; Yan, X.; Xu, Y.Y.; Yoza, B.A.; Wang, X.; Kou, Y.; Ye, H.; Wang, Q.; Li, Q.X. Activated petroleum waste sludge biochar for efficient catalytic ozonation of refinery wastewater. *Sci. Total Environ.* **2019**, *651*, 2631–2640. [CrossRef]

78. Wang, J.; Chen, S.; Quan, X.; Yu, H. Fluorine-doped carbon nanotubes as an efficient metal-free catalyst for destruction of organic pollutants in catalytic ozonation. *Chemosphere* **2018**, *190*, 135–143. [CrossRef]

79. Sun, Z.; Zhao, L.; Liu, C.; Zhen, Y.; Ma, J. Catalytic Ozonation of Ketoprofen with In Situ N-Doped Carbon: A Novel Synergetic Mechanism of Hydroxyl Radical Oxidation and an Intra-Electron-Transfer Nonradical Reaction. *Environ. Sci. Technol.* **2019**, *53*, 10342–10351. [CrossRef]

80. Oh, W.D.; Dong, Z.; Lim, T.T. Generation of sulfate radical through heterogeneous catalysis for organic contaminants removal: Current development, challenges and prospects. *Appl. Catal. B Environ.* **2016**, *194*, 169–201. [CrossRef]

81. Gao, H.Y.; Huang, C.H.; Mao, L.; Shao, B.; Shao, J.; Yan, Z.Y.; Tang, M.; Zhu, B.Z. First Direct and Unequivocal Electron Spin Resonance Spin-Trapping Evidence for pH-Dependent Production of Hydroxyl Radicals from Sulfate Radicals. *Environ. Sci. Technol.* **2020**, *54*, 14046–14056. [CrossRef]

82. Ding, D.; Zhou, L.; Kang, F.; Yang, S.; Chen, R.; Cai, T.; Duan, X.; Wang, S. Synergistic Adsorption and Oxidation of Ciprofloxacin by Biochar Derived from Metal-Enriched Phytoremediation Plants: Experimental and Computational Insights. *ACS Appl. Mater. Interfaces* **2020**, *12*, 53788–53798. [CrossRef] [PubMed]

83. Wan, Z.; Xu, Z.; Sun, Y.; He, M.; Hou, D.; Cao, X.; Tsang, D.C.W. Critical Impact of Nitrogen Vacancies in Nonradical Carbocatalysis on Nitrogen-Doped Graphitic Biochar. *Environ. Sci. Technol.* **2021**, *55*, 7004–7014. [CrossRef] [PubMed]

84. Du, L.; Xu, W.; Liu, S.; Li, X.; Huang, D.; Tan, X.; Liu, Y. Activation of persulfate by graphitized biochar for sulfamethoxazole removal: The roles of graphitic carbon structure and carbonyl group. *J. Colloid Interface Sci.* **2020**, *577*, 419–430. [CrossRef]

85. Huang, B.C.; Jiang, J.; Huang, G.X.; Yu, H.Q. Sludge biochar-based catalysts for improved pollutant degradation by activating peroxymonosulfate. *J. Mater. Chem. A* **2018**, *6*, 8978–8985. [CrossRef]

86. Hu, Y.; Chen, D.; Zhang, R.; Ding, Y.; Ren, Z.; Fu, M.; Cao, X.; Zeng, G. Singlet oxygen-dominated activation of peroxymonosulfate by passion fruit shell derived biochar for catalytic degradation of tetracycline through a non-radical oxidation pathway. *J. Hazard. Mater.* **2021**, *419*, 126495. [CrossRef] [PubMed]

87. Sun, C.; Chen, T.; Huang, Q.; Zhan, M.; Li, X.; Yan, J. Activation of persulfate by CO₂-activated biochar for improved phenolic pollutant degradation: Performance and mechanism. *Chem. Eng. J.* **2020**, *380*, 122519. [CrossRef]

88. Qi, Y.; Ge, B.; Zhang, Y.; Jiang, B.; Wang, C.; Akram, M.; Xu, X. Three-dimensional porous graphene-like biochar derived from Enteromorpha as a persulfate activator for sulfamethoxazole degradation: Role of graphitic N and radicals transformation. *J. Hazard. Mater.* **2020**, *399*, 123039. [CrossRef]

89. Zou, J.; Yu, J.; Tang, L.; Ren, X.; Pang, Y.; Zhang, H.; Xie, Q.; Liu, Y.; Liu, H.; Luo, T. Analysis of reaction pathways and catalytic sites on metal-free porous biochar for persulfate activation process. *Chemosphere* **2020**, *261*, 127747. [CrossRef]

90. Wang, X.; Zhang, P.; Wang, C.; Jia, H.; Shang, X.; Tang, J.; Sun, H. Metal-rich hyperaccumulator-derived biochar as an efficient persulfate activator: Role of intrinsic metals (Fe, Mn and Zn) in regulating characteristics, performance and reaction mechanisms. *J. Hazard. Mater.* **2021**, *424*, 127225. [CrossRef]

91. Ouyang, D.; Chen, Y.; Yan, J.; Qian, L.; Han, L.; Chen, M. Activation mechanism of peroxymonosulfate by biochar for catalytic degradation of 1,4-dioxane: Important role of biochar defect structures. *Chem. Eng. J.* **2019**, *370*, 614–624. [CrossRef]

92. Zhu, S.; Huang, X.; Ma, F.; Wang, L.; Duan, X.; Wang, S. Catalytic Removal of Aqueous Contaminants on N-Doped Graphitic Biochars: Inherent Roles of Adsorption and Nonradical Mechanisms. *Environ. Sci. Technol.* **2018**, *52*, 8649–8658. [CrossRef] [PubMed]

93. Ma, W.; Wang, N.; Du, Y.; Xu, P.; Sun, B.; Zhang, L.; Lin, K.Y.A. Human-Hair-Derived N, S-Doped Porous Carbon: An Enrichment and Degradation System for Wastewater Remediation in the Presence of Peroxymonosulfate. *ACS Sustain. Chem. Eng.* **2019**, *7*, 2718–2727. [CrossRef]

94. Xu, Y.; Liu, S.; Wang, M.; Zhang, J.; Ding, H.; Song, Y.; Zhu, Y.; Pan, Q.; Zhao, C.; Deng, H. Thiourea-assisted one-step fabrication of a novel nitrogen and sulfur co-doped biochar from nanocellulose as metal-free catalyst for efficient activation of peroxymonosulfate. *J. Hazard. Mater.* **2021**, *416*, 125796. [CrossRef] [PubMed]

95. Oh, W.-D.; Jannah Zaeni, J.R.; Lisak, G.; Andrew Lin, K.-Y.; Leong, K.-H.; Choong, Z.-Y. Accelerated organics degradation by peroxymonosulfate activated with biochar co-doped with nitrogen and sulfur. *Chemosphere* **2021**, *277*, 130313. [CrossRef] [PubMed]

96. Fang, G.; Liu, C.; Gao, J.; Dionysiou, D.D.; Zhou, D. Manipulation of persistent free radicals in biochar to activate persulfate for contaminant degradation. *Environ. Sci. Technol.* **2015**, *49*, 5645–5653. [CrossRef]

97. Zhang, Y.; Xu, M.; Liang, S.; Feng, Z.; Zhao, J. Mechanism of persulfate activation by biochar for the catalytic degradation of antibiotics: Synergistic effects of environmentally persistent free radicals and the defective structure of biochar. *Sci. Total Environ.* **2021**, *794*, 148707. [CrossRef]

98. Liu, J.; Huang, S.; Wang, T.; Mei, M.; Chen, S.; Li, J. Peroxydisulfate activation by digestate-derived biochar for azo dye degradation: Mechanism and performance. *Sep. Purif. Technol.* **2021**, *279*, 119687. [CrossRef]

99. Jin, Z.; Xiao, S.; Dong, H.; Xiao, J.; Tian, R.; Chen, J.; Li, Y.; Li, L. Adsorption and catalytic degradation of organic contaminants by biochar: Overlooked role of biochar's particle size. *J. Hazard. Mater.* **2022**, *422*, 126928. [CrossRef]

100. Chen, Y.P.; Zheng, C.H.; Huang, Y.Y.; Chen, Y.R. Removal of chlortetracycline from water using spent tea leaves-based biochar as adsorption-enhanced persulfate activator. *Chemosphere* **2022**, *286*, 131770. [CrossRef]

101. Wang, Y.; Song, Y.; Li, N.; Liu, W.; Yan, B.; Yu, Y.; Liang, L.; Chen, G.; Hou, L.; Wang, S. Tunable active sites on biogas digestate derived biochar for sulfanilamide degradation by peroxymonosulfate activation. *J. Hazard. Mater.* **2022**, *421*, 126794. [CrossRef]

102. Zhong, Q.; Lin, Q.; He, W.; Fu, H.; Huang, Z.; Wang, Y.; Wu, L. Study on the nonradical pathways of nitrogen-doped biochar activating persulfate for tetracycline degradation. *Sep. Purif. Technol.* **2021**, *276*, 119354. [CrossRef]

103. Avramiotis, E.; Frontistis, Z.; Manariotis, I.D.; Vakros, J.; Mantzavinos, D. Oxidation of Sulfamethoxazole by Rice Husk Biochar-Activated Persulfate. *Catalysts* **2021**, *11*, 850. [CrossRef]

104. Abdellah, M.H.; Nosier, S.A.; El-Shazly, A.H.; Mubarak, A.A. Photocatalytic decolorization of methylene blue using TiO_2/UV system enhanced by air sparging. *Alex. Eng. J.* **2018**, *57*, 3727–3735. [CrossRef]

105. Byrne, J.A.; Dunlop, P.S.M.; Hamilton, J.W.J.; Fernández-Ibáñez, P.; Polo-López, I.; Sharma, P.K.; Vennard, A.S.M. A review of heterogeneous photocatalysis for water and surface disinfection. *Molecules* **2015**, *20*, 5574–5615. [CrossRef] [PubMed]

106. Mahlambi, M.; Ngila, C.; Mamba, B. Recent Developments in Environmental Photocatalytic Degradation of Organic Pollutants: The Case of Titanium Dioxide Nanoparticles-A Review. *J. Nanomater.* **2015**, *2015*, 790173. [CrossRef]

107. Arimi, A.; Günnemann, C.; Curti, M.; Bahnemann, W.D. Regarding the Nature of Charge Carriers Formed by UV or Visible Light Excitation of Carbon-Modified Titanium Dioxide. *Catalysts* **2019**, *9*, 697. [CrossRef]

108. Pirhashemi, M.; Habibi-Yangjeh, A. Preparation of novel nanocomposites by deposition of Ag_2WO_4 and AgI over ZnO particles: Efficient plasmonic visible-light-driven photocatalysts through a cascade mechanism. *Ceram. Int.* **2017**, *43*, 13447–13460. [CrossRef]

109. Rashid, J.; Parveen, N.; Iqbal, A.; Awan, S.U.; Iqbal, N.; Talib, S.H.; Hussain, N.; Akram, B.; Ulhaq, A.; Ahmed, B.; et al. Facile synthesis of g-C3N4(0.94)/CeO2(0.05)/Fe3O4(0.01) nanosheets for DFT supported visible photocatalysis of 2-Chlorophenol. *Sci. Rep.* **2019**, *9*, 10202. [CrossRef]

110. Chen, N.; Huang, Y.; Hou, X.; Ai, Z.; Zhang, L. Photochemistry of Hydrochar: Reactive Oxygen Species Generation and Sulfadimidine Degradation. *Environ. Sci. Technol.* **2017**, *51*, 11278–11287. [CrossRef]

111. Fang, G.; Liu, C.; Wang, Y.; Dionysiou, D.D.; Zhou, D. Photogeneration of reactive oxygen species from biochar suspension for diethyl phthalate degradation. *Appl. Catal. B Environ.* **2017**, *214*, 34–45. [CrossRef]

112. Xiao, Y.; Lyu, H.; Tang, J.; Wang, K.; Sun, H. Effects of ball milling on the photochemistry of biochar: Enrofloxacin degradation and possible mechanisms. *Chem. Eng. J.* **2020**, *384*, 123311. [CrossRef]

113. Chen, X.; Oh, W.D.; Lim, T.T. Graphene- and CNTs-based carbocatalysts in persulfates activation: Material design and catalytic mechanisms. *Chem. Eng. J.* **2018**, *354*, 941–976. [CrossRef]

114. Ejaz, A.; Jeon, S. The individual role of pyrrolic, pyridinic and graphitic nitrogen in the growth kinetics of Pd NPs on N-rGO followed by a comprehensive study on ORR. *Int. J. Hydrogen Energy* **2018**, *43*, 5690–5702. [CrossRef]

115. Tetteh, E.K.; Rathilal, S.; Naidoo, D.B. Photocatalytic degradation of oily waste and phenol from a local South Africa oil refinery wastewater using response methodology. *Sci. Rep.* **2020**, *10*, 8850. [CrossRef]

116. Van de Moortel, W.; Kamali, M.; Sniegowski, K.; Braeken, L.; Degrève, J.; Luyten, J.; Dewil, R. How photocatalyst dosage and ultrasound application influence the photocatalytic degradation rate of phenol in water: Elucidating the mechanisms behind. *Water* **2020**, *12*, 1672. [CrossRef]

117. Lee, J.; Von Gunten, U.; Kim, J.H. Persulfate-Based Advanced Oxidation: Critical Assessment of Opportunities and Roadblocks. *Environ. Sci. Technol.* **2020**, *54*, 3064–3081. [CrossRef]

118. Wang, S.; Wang, J. Kinetics of PMS activation by graphene oxide and biochar. *Chemosphere* **2020**, *239*, 124812. [CrossRef]

119. Ambaye, T.G.; Vaccari, M.; van Hullebusch, E.D.; Amrane, A.; Rtimi, S. Mechanisms and adsorption capacities of biochar for the removal of organic and inorganic pollutants from industrial wastewater. *Int. J. Environ. Sci. Technol.* **2020**, *18*, 3273–3294. [CrossRef]

120. Zaimee, M.Z.A.; Sarjadi, M.S.; Rahman, M.L. Heavy Metals Removal from Water by Efficient Adsorbents. *Water* **2021**, *13*, 2659. [CrossRef]

121. Guo, X.; Liu, A.; Lu, J.; Niu, X.; Jiang, M.; Ma, Y.; Liu, X.; Li, M. Adsorption Mechanism of Hexavalent Chromium on Biochar: Kinetic, Thermodynamic, and Characterization Studies. *ACS Omega* **2020**, *5*, 27323–27331. [CrossRef]

122. Chen, N.; Fang, G.; Zhu, C.; Wu, S.; Liu, G.; Dionysiou, D.D.; Wang, X.; Gao, J.; Zhou, D. Surface-bound radical control rapid organic contaminant degradation through peroxymonosulfate activation by reduced Fe-bearing smectite clays. *J. Hazard. Mater.* **2020**, *389*, 121819. [CrossRef] [PubMed]

123. Ding, Y.; Wang, X.; Fu, L.; Peng, X.; Pan, C.; Mao, Q.; Wang, C.; Yan, J. Nonradicals induced degradation of organic pollutants by peroxydisulfate (PDS) and peroxymonosulfate (PMS): Recent advances and perspective. *Sci. Total Environ.* **2020**, *765*, 142794. [CrossRef] [PubMed]

124. Tomczyk, A.; Sokołowska, Z.; Boguta, P. Biochar physicochemical properties: Pyrolysis temperature and feedstock kind effects. *Rev. Environ. Sci. Biotechnol.* **2020**, *19*, 191–215. [CrossRef]

125. Yu, J.; Zhu, Z.; Zhang, H.; Shen, X.; Qiu, Y.; Yin, D.; Wang, S. Persistent free radicals on N-doped hydrochar for degradation of endocrine disrupting compounds. *Chem. Eng. J.* **2020**, *398*, 125538. [CrossRef]

126. Xu, L.; Wu, C.; Chai, C.; Cao, S.; Bai, X.; Ma, K.; Jin, X.; Shi, X.; Jin, P. Adsorption of micropollutants from wastewater using iron and nitrogen co-doped biochar: Performance, kinetics and mechanism studies. *J. Hazard. Mater.* **2021**, *424*, 127606. [CrossRef]

127. Li, X.; Zhang, S.; Yu, M.; Xu, H.; Lv, J.; Yang, S.; Zhu, X.; Li, L. One-pot pyrolysis method for synthesis of Fe/N co-doped biochar as an effective peroxymonosulfate activator for RhB degradation. *J. Taiwan Inst. Chem. Eng.* **2021**, *128*, 209–219. [CrossRef]

128. Guerra-Rodríguez, S.; Rodríguez, E.; Singh, D.N.; Rodríguez-Chueca, J. Assessment of sulfate radical-based advanced oxidation processes for water and wastewater treatment: A review. *Water* **2018**, *10*, 1828. [CrossRef]

129. Qin, Y.; Li, X.; Wang, L.; Luo, J.; Li, Y.; Yao, C.; Xiao, Z.; Zhai, S.; An, Q. Valuable cobalt/biochar with enriched surface oxygen-containing groups prepared from bio-waste shrimp shell for efficient peroxymonosulfate activation. *Sep. Purif. Technol.* **2022**, *281*, 119901. [CrossRef]

130. Hou, J.; Xu, L.; Han, Y.; Tang, Y.; Wan, H.; Xu, Z.; Zheng, S. Deactivation and regeneration of carbon nanotubes and nitrogen-doped carbon nanotubes in catalytic peroxymonosulfate activation for phenol degradation: Variation of surface functionalities. *RSC Adv.* **2019**, *9*, 974–983. [CrossRef]

131. Poulose, A.M.; Elnour, A.Y.; Anis, A.; Shaikh, H.; Al-Zahrani, S.M.; George, J.; Al-Wabel, M.I.; Usman, A.R.; Ok, Y.S.; Tsang, D.C.W.; et al. Date palm biochar-polymer composites: An investigation of electrical, mechanical, thermal and rheological characteristics. *Sci. Total Environ.* **2018**, *619–620*, 311–318. [CrossRef]

132. Das, C.; Tamrakar, S.; Kiziltas, A.; Xie, X. Incorporation of Biochar to Improve Mechanical, Thermal and Electrical Properties of Polymer Composites. *Polymers* **2021**, *13*, 2663. [CrossRef] [PubMed]

133. Iqbal, A.; Saidu, U.; Adam, F.; Sreekantan, S.; Yahaya, N.; Ahmad, M.N.; Ramalingam, R.J.; Wilson, L.D. Floating ZnO QDs-Modified TiO_2/LLDPE Hybrid Polymer Film for the Effective Photodegradation of Tetracycline under Fluorescent Light Irradiation: Synthesis and Characterisation. *Molecules* **2021**, *26*, 2509. [CrossRef] [PubMed]

134. Abdul-Rahman, N.R.; Muniandy, L.; Adam, F.; Iqbal, A.; Ng, E.P.; Lee, H.L. Detailed photocatalytic study of alkaline titanates and its application for the degradation of methylene blue (MB) under solar irradiation. *J. Photochem. Photobiol. A Chem.* **2019**, *375*, 219–230. [CrossRef]

135. Venieri, D.; Mantzavinos, D.; Binas, V. Solar Photocatalysis for Emerging Micro-Pollutants Abatement and Water Disinfection: A Mini-Review. *Sustainability* **2020**, *12*, 10047. [CrossRef]

136. Huang, H.; Pradhan, B.; Hofkens, J.; Roeffaers, M.B.J.; Steele, J.A. Solar-Driven Metal Halide Perovskite Photocatalysis: Design, Stability, and Performance. *ACS Energy Lett.* **2020**, *5*, 1107–1123. [CrossRef]

137. Dharwadkar, S.; Yu, L.; Achari, G. Photocatalytic Degradation of Sulfolane Using a LED-Based Photocatalytic Treatment System. *Catalysts* **2021**, *11*, 624. [CrossRef]

138. Casado, C.; Timmers, R.; Sergejevs, A.; Clarke, C.T.; Allsopp, D.W.E.; Bowen, C.R.; van Grieken, R.; Marugán, J. Design and validation of a LED-based high intensity photocatalytic reactor for quantifying activity measurements. *Chem. Eng. J.* **2017**, *327*, 1043–1055. [CrossRef]

139. Li, X.; Li, Z.; Xing, Z.; Song, Z.; Ye, B.; Wang, Z.; Wu, Q. UV-LED/P25-based photocatalysis for effective degradation of isothiazolone biocide. *Front. Environ. Sci. Eng.* **2020**, *15*, 85. [CrossRef]

140. Faisal, M.; Iqbal, A.; Adam, F.; Jothiramalingam, R. Effect of Cu doping on the photocatalytic activity of InVO4 for hazardous dye photodegradation under LED light and its mechanism. *Water Sci. Technol.* **2021**, *84*, 576–595. [CrossRef]

141. Jo, W.K.; Tayade, R.J. New generation energy-efficient light source for photocatalysis: LEDs for environmental applications. *Ind. Eng. Chem. Res.* **2014**, *53*, 2073–2084. [CrossRef]

142. Mundy, B.; Kuhnel, B.; Hunter, G.; Jarnis, R.; Funk, D.; Walker, S.; Burns, N.; Drago, J.; Nezgod, W.; Huang, J.; et al. A Review of Ozone Systems Costs for Municipal Applications. Report by the Municipal Committee—IOA Pan American Group. *Ozone Sci. Eng.* **2018**, *40*, 266–274. [CrossRef]

143. Xiao, T.; Dai, X.; Wang, X.; Chen, S.; Dong, B. Enhanced sludge dewaterability via ozonation catalyzed by sludge derived biochar loaded with $MnFe_2O_4$: Performance and mechanism investigation. *J. Clean. Prod.* **2021**, *323*, 129182. [CrossRef]